

# Emergent spin-resolved electronic charge density waves and pseudogap phenomena from strong $d$ -wave altermagnetism

Fei Yang,<sup>1,\*</sup> Guo-Dong Zhao,<sup>1</sup> Binghai Yan,<sup>2</sup> and Long-Qing Chen<sup>1,†</sup>

<sup>1</sup>*Department of Materials Science and Engineering and Materials Research Institute, The Pennsylvania State University, University Park, PA 16802, USA*

<sup>2</sup>*Department of Physics, The Pennsylvania State University, University Park, PA 16802, USA*

(Dated: February 13, 2026)

Inspired by recent discovery of metallic  $d$ -wave altermagnetism in  $\text{KV}_2\text{Se}_2\text{O}$ , we develop a self-consistent microscopic many-body calculation of density-wave order for an itinerant altermagnetic metal. We show that the strong  $d$ -wave spin-momentum locking inherent to the altermagnetic band structure reconstructs the Fermi surface into spin-selective quasi-1D open sheets. This unique topology of Fermi surface drives an instability toward spin-resolved electronic charge density waves (CDWs), in which the ordering wave vectors for spin-up and spin-down electrons condense along two mutually orthogonal directions, forming spin-resolved stripe phases. As a consequence, this results in pronounced gap openings near the Fermi surface, and the superposition of these spin-resolved stripe orders leads to a checkerboard CDW in the charge channel and an antiphase spin-density-wave modulation in the spin channel. Upon increasing temperature, the density-wave order melts at  $T_c$  due to thermal phase fluctuation while the gap opening persists, giving rise to a robust pseudogap regime, which eventually closes at a higher temperature  $T_g$ . The resulting simulations quantitatively reproduce the key features observed in the spectroscopic measurements, offering a consistent and generic understanding of the reported phenomena in  $\text{KV}_2\text{Se}_2\text{O}$  and, more broadly, in metallic altermagnets with strong spin-momentum locking.

**Introduction.**—Over the past few years, altermagnetism has been identified as a distinct form of magnetic order that lies outside the conventional ferromagnetic–antiferromagnetic dichotomy [1–7]. In altermagnets, oppositely spin-polarized electronic states reside on symmetry-related sublattices connected by crystalline rotations. As a result, the time-reversal symmetry is broken without generating a macroscopic magnetization [1–3]. A defining hallmark of altermagnetism is the emergence of an even-parity, momentum-dependent spin splitting that remains compatible with inversion symmetry. This splitting originates from symmetry-enforced band degeneracies and typically exhibits higher-angular-momentum form factors, such as  $d$ -,  $g$ -, or even  $i$ -wave structures [1, 2]. This unique symmetry-protected spin splitting in altermagnets gives rise to highly anisotropic, spin-resolved electronic dispersions, making these systems particularly attractive for spintronic applications [8–13] as well as emerging quantum-transport [14–18] or superconductivity-based [19–25] technologies.

Early material realizations of strong altermagnetism, such as  $\text{MnTe}$  [26–28] and  $\text{MnTe}_2$  [29], were predominantly semiconducting, limiting the role of the electronic many-body effects. The magnetic nature of  $\text{RuO}_2$ , although proposed as a metallic altermagnetic candidate, remains under active debate [30, 31]. Very recently, the compound  $\text{KV}_2\text{Se}_2\text{O}$  has been identified as a metallic, room-temperature  $d$ -wave altermagnet [32–36], supported by a combination of spin- and angle-resolved photoemission spectroscopy (ARPES) [32], nuclear magnetic resonance (NMR) [32], and density-functional-theory (DFT) calculations [33–36]. A striking feature revealed by these studies is the exceptionally strong momentum-dependent spin splitting of the metallic bands: for one spin sector the dispersion has opposite curvatures along two orthogonal crystallographic directions, while the opposite pattern occurs for the other spin sector. This leads to open, quasi-one-dimensional (1D) Fermi-

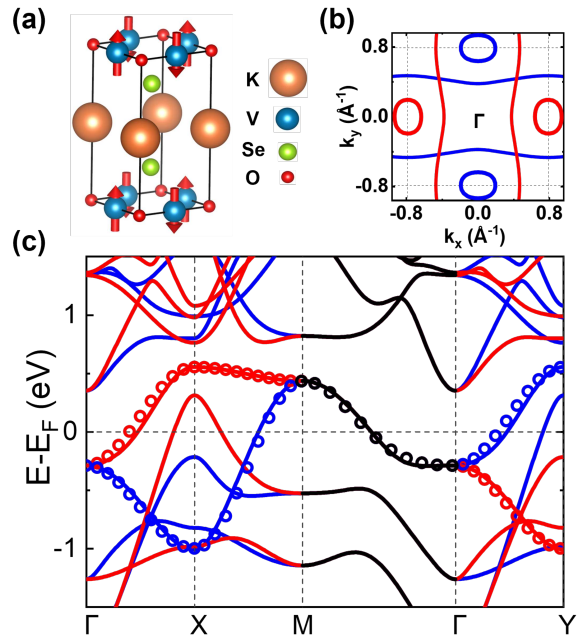


FIG. 1. Atomic and electronic structure of  $\text{KV}_2\text{Se}_2\text{O}$  calculated by DFT. (a) Crystal unit cell of  $\text{KV}_2\text{Se}_2\text{O}$ , where red arrows indicates the spin states. (b) Fermi surface at the  $k_z = 0$  plane, where the red and blue curves corresponds to spin-up and spin-down states, respectively. (c) Band structure without spin-orbit coupling. Red, blue, and black curves denote spin-up, spin-down, and spin-degenerate bands, respectively. The circles represent results from the tight-binding model, shown in the same color scheme as the DFT bands.

surface sheets that are spin selective, as illustrated in Fig. 1(b).

Such quasi-1D Fermi-surface sheets in an itinerant electronic system naturally suggests a generically enhanced susceptibility to collective ordering. Experimentally, NMR spec-

tra of  $\text{KV}_2\text{Se}_2\text{O}$  [32] reveal a transition from a uniform magnetic response at high temperatures to a distinct spectral splitting upon cooling below 100 K, indicating the emergence of an ordered phase. Meanwhile, ARPES measurements [32] reveal pronounced gap openings along the  $\Gamma$ -X and X/Y-M directions of the Brillouin zone. The low-temperature phase is then attributed, in several DFT studies [32, 34, 36], to a spin-density-wave (SDW) instability with an ordering vector  $Q_0 = (\pi/a, \pi/a)$ . Interestingly, the gap opening was experimentally found to persist up to 230 K [32], far above the ordering temperature 100 K, and is interpreted as a pseudogap regime whose microscopic origin remains unresolved.

From a more general theoretical perspective, quasi-1D electronic structures are generically more prone to charge-density-wave (CDW) instabilities [37–43]. In particular, the appearance of pseudogaps typically points to the emergence of electronic condensation, beyond a purely single-particle picture as captured by standard DFT calculations. In this work, we develop a self-consistent microscopic many-body calculation of density-wave order for an itinerant  $d$ -wave altermagnetic metal and demonstrate that the dominant electronic instability takes the form of spin-resolved CDW order. We show that spin-up and spin-down electrons condense at two mutually orthogonal ordering wave vectors, producing stripe-like modulations in each spin sector. This composite order leads to substantial single-particle gap openings around the Fermi surface along the  $\Gamma$ -X/Y and X/Y-M directions. Remarkably, the superposition of these orthogonal spin-resolved stripe orders generates a checkerboard CDW in the charge channel, accompanied by an antiphase SDW modulation in the spin channel. Going beyond mean-field theory at the self-consistent microscopic level, we further determine the finite-temperature behaviors and phase transitions. Upon heating, density-wave order melts at a critical temperature  $T_c$  due to bosonic thermal phase fluctuations, while the single-particle gap openings remain robust, giving rise to an extended pseudogap regime that closes only at a higher temperature  $T_g$ . Our results quantitatively reproduce key spectroscopic features and transition temperatures observed experimentally [32]. We therefore conclude that the composite spin-resolved CDW order constitutes a natural and generic instability of the metallic  $d$ -wave altermagnets.

*Model.*—The band structure and the related Fermi surface of compound  $\text{KV}_2\text{Se}_2\text{O}$  obtained from our DFT calculations [44–46] is shown in Fig. 1. Despite being metallic,  $\text{KV}_2\text{Se}_2\text{O}$  exhibits a pronounced  $d$ -wave momentum-dependent spin splitting throughout the Brillouin zone [Fig. 1(c)]: for the spin-up channel, the band curvature is positive along  $\Gamma$ -X but negative along  $\Gamma$ -Y, and the opposite behavior is found for the spin-down one, whereas the bands remain spin degenerate along  $\Gamma$ -M. As a result, the two metallic bands form spin-resolved quasi-1D Fermi-surface sheets oriented along two orthogonal directions [Fig. 1(b)], while additional spin-polarized hole pockets appear at the X and Y points.

Motivated by both experimental observation [32] and theoretical expectation [37–40] that the density-wave ordering tendencies are primarily governed by the quasi-1D Fermi-surface

sheets, we start with a standard interacting Hamiltonian [41],

$$H = \sum_{\mathbf{k}, s} \xi_{\mathbf{k}, s} c_{\mathbf{k}s}^\dagger c_{\mathbf{k}s} + \frac{1}{2} \sum_{\mathbf{k}\mathbf{k}'\mathbf{q}, ss'} U(\mathbf{q}) c_{\mathbf{k}+\mathbf{q}s}^\dagger c_{\mathbf{k}s} c_{\mathbf{k}'s'}^\dagger c_{\mathbf{k}'+\mathbf{q}s'}, \quad (1)$$

where  $c_{\mathbf{k}s}^\dagger$  and  $c_{\mathbf{k}s}$  denote creation and annihilation operators for an electron with momentum  $\mathbf{k}$  and spin  $s$ . The tight-binding dispersion is given by [47]  $\xi_{\mathbf{k}, s} = -2t(\cos k_x + \cos k_y) - 4t' \cos k_x \cos k_y - 2t_j s_z (\cos k_x - \cos k_y) - \mu$ , where  $t$  and  $t'$  are the nearest- and next-nearest-neighbor hopping amplitudes, and  $t_j$  parametrizes the  $d$ -wave momentum-dependent spin splitting induced by altermagnetism. As seen from Fig. 1(c), via a simple parameter fitting, this tight-binding model faithfully captures the key features of the DFT band structure of the relevant bands. The interaction term  $U(\mathbf{q})$  describes the effective spin-conserving electron-electron interactions. Following standard practice in formulating density-wave order [41–43], we assume momentum-independent couplings in the relevant density-wave channels and take  $U(\mathbf{Q}_s) = V/4$ .

The density-wave order is favored in systems with nested Fermi surfaces, i.e., different parts of the Fermi surface are connected by the vector  $\mathbf{Q}$  such that  $\xi_{\mathbf{k}+\mathbf{Q}} = -\xi_{\mathbf{k}}$ . Clearly, the two spin sectors exhibit distinct nesting conditions due to the strongly spin-resolved quasi-1D band structure induced by the  $d$ -wave altermagnetism. We therefore allow spin-up and spin-down electrons to condense at different ordering wave vectors  $\mathbf{Q}_s$ , naturally chosen to connect the two open Fermi-surface sheets for each spin sector [Fig. 1(b)]. For a given spin- $s$  sector, the separation between the two inversion-related open Fermi sheets at polar angle  $\theta$  is  $2k_F^s(\theta)$ , so one has

$$\mathbf{Q}_s = 2k_F^s(\theta_{\mathbf{Q}_s}) (\cos \theta_{\mathbf{Q}_s} \hat{\mathbf{e}}_x + \sin \theta_{\mathbf{Q}_s} \hat{\mathbf{e}}_y). \quad (2)$$

The optimal  $\mathbf{Q}_s^{\text{op}}$  is ultimately determined by maximizing the available phase space for pairing. Specifically, singling out the ordering wave vector  $\mathbf{q} = \mathbf{Q}_s$  in the interaction term of Hamiltonian (1), the mean-field decoupling in the density-wave channel yields spin-resolved order parameters,

$$\Delta_{\mathbf{Q}_s} = \frac{V}{2} \sum_{\mathbf{k}} \langle c_{\mathbf{k}+\mathbf{Q}_s s}^\dagger c_{\mathbf{k}s} \rangle, \quad \Delta_{\mathbf{Q}_s}^* = \frac{V}{2} \sum_{\mathbf{k}} \langle c_{\mathbf{k}s}^\dagger c_{\mathbf{k}+\mathbf{Q}_s s} \rangle, \quad (3)$$

and the resulting mean-field Hamiltonian can be written as

$$H_{\text{MF}} = \sum_s \frac{1}{2} \sum_{\mathbf{k}} (c_{\mathbf{k}s}^\dagger, c_{\mathbf{k}+\mathbf{Q}_s s}^\dagger) \begin{pmatrix} \xi_{\mathbf{k}, s} & \Delta_{\mathbf{Q}_s} \\ \Delta_{\mathbf{Q}_s}^* & \xi_{\mathbf{k}+\mathbf{Q}_s, s} \end{pmatrix} \begin{pmatrix} c_{\mathbf{k}s} \\ c_{\mathbf{k}+\mathbf{Q}_s s} \end{pmatrix} - |\Delta_{\mathbf{Q}_s}|^2 / V - |\Delta_{\mathbf{Q}_s^*}|^2 / V. \quad (4)$$

Diagonalizing this BCS-like mean-field Hamiltonian  $H_{\text{MF}}$ , we obtain the spin-resolved quasiparticle excitation spectrum,

$$E_{\mathbf{k}s}^\pm = \frac{\xi_{\mathbf{k}, s} + \xi_{\mathbf{k}+\mathbf{Q}_s, s}}{2} \pm \sqrt{\left( \frac{\xi_{\mathbf{k}, s} - \xi_{\mathbf{k}+\mathbf{Q}_s, s}}{2} \right)^2 + |\Delta_{\mathbf{Q}_s}|^2}, \quad (5)$$

and the self-consistent gap equation takes the form (Sec. SII):

$$\frac{1}{V} = \frac{1}{2} \sum_{\mathbf{k}} \frac{f(E_{\mathbf{k}s}^-) - f(E_{\mathbf{k}s}^+)}{2E_{\mathbf{k}s}}, \quad (6)$$

where  $E_{\mathbf{k}s} = \sqrt{[(\xi_{\mathbf{k},s} - \xi_{\mathbf{k}+\mathbf{Q}_s,s})/2]^2 + |\Delta_{\mathbf{Q}_s}|^2}$  and  $f(x)$  is the Fermi-Dirac distribution function.

By solving self-consistently Eqs. (5) and (6), one can determine the spin-resolved density-wave gaps  $|\Delta_{\mathbf{Q}_s}|$  as functions of the ordering direction  $\theta_{\mathbf{Q}_s}$ . The optimal orientation  $\theta_{\mathbf{Q}_s}$  is selected by minimizing the mean-field free energy with respect to  $\theta_{\mathbf{Q}_s}$ . Equivalently, within mean-field theory, this procedure amounts to choosing the direction that yields the largest self-consistent gap magnitude,  $|\Delta_s| = |\Delta_{\mathbf{Q}_s}(\theta_{\mathbf{Q}_s})|_{\max}$ , which fixes  $\theta_{\mathbf{Q}_s}$  and hence selects the optimal ordering wave vector  $\mathbf{Q}_s^{\text{op}}$  for each spin sector. Details of the numerical-simulation treatments are provided in the Supplemental Materials (Sec. SIV). The interaction strength  $V$  is fixed to reproduce the experimentally observed gap magnitude  $|\Delta_s(T \sim 0)| = 35$  meV [32].

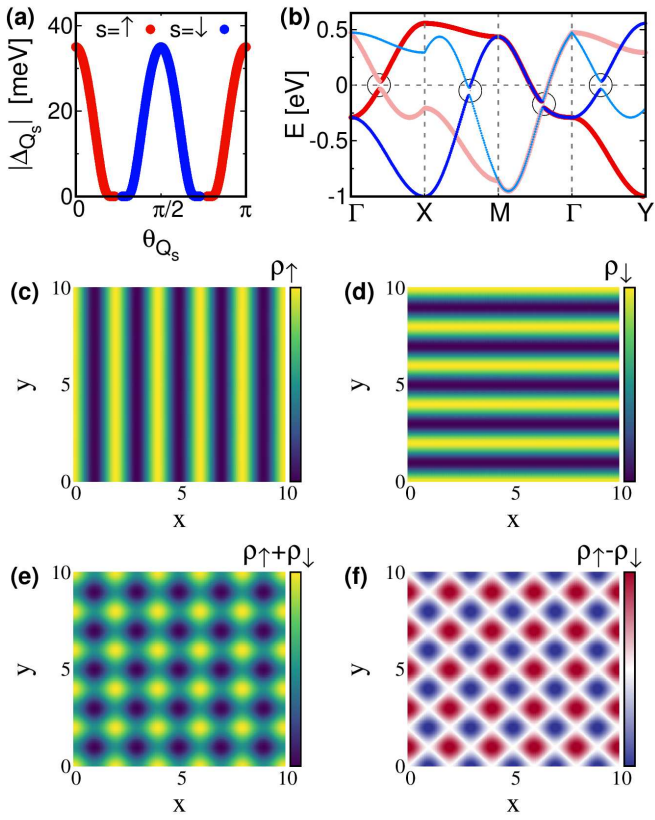


FIG. 2. (a) Self-consistently calculated spin-resolved density-wave gap magnitudes  $|\Delta_{\mathbf{Q}_s}|$  as functions of the ordering direction  $\theta_{\mathbf{Q}_s}$ . (b) Quasiparticle energy spectra in the density-wave state, showing the gap opening around the Fermi surface. Red (blue) curves denote the spin-up (spin-down) bands. The darker curves represent the original quasiparticle dispersion with the gap opening, whereas the lighter curves correspond to the backfolded bands arising from particle-hole mixing induced by the density-wave order. The black dashed circles highlight the gapped regions on the Fermi surface. (c) and (d) Real-space density modulations  $\rho_{\uparrow}$  and  $\rho_{\downarrow}$  associated with the spin-up and spin-down density-wave orders, respectively. (e) Total charge-density modulation  $\rho_{\uparrow} + \rho_{\downarrow}$ . (f) Spin-density modulation  $\rho_{\uparrow} - \rho_{\downarrow}$  [see Sec. SVII for more details of its incommensurate nature (Fig. SI)].

*Ground State.*—The numerical results for the  $T = 0$  ground state are shown in Fig. 2. As seen from Fig. 2(a), the spin-

resolved gap magnitudes  $|\Delta_{\mathbf{Q}_\uparrow}(\theta_{\mathbf{Q}_\uparrow})|$  and  $|\Delta_{\mathbf{Q}_\downarrow}(\theta_{\mathbf{Q}_\downarrow})|$  reach their maxima at  $\theta_{\mathbf{Q}_\uparrow} = 0$  and  $\theta_{\mathbf{Q}_\downarrow} = \pi/2$ , respectively. Away from the optimal orientation, the gap magnitude decreases rapidly, indicating a strong angular selectivity of the density-wave ordering. The underlying key reason is that the two open Fermi sheets for each spin are nearly parallel [Fig. 1(b)], so that density-wave ordering is sharply selected along the nesting (quasi-1D-transport) direction as expected, consistent with the established 1D instability of electronic systems [37–43].

The optimal ordering wave vector for each spin sector from Fig. 2(a),  $\mathbf{Q}_\uparrow^{\text{op}} = 2k_F^\uparrow(\theta = 0)\mathbf{e}_x$  and  $\mathbf{Q}_\downarrow^{\text{op}} = 2k_F^\downarrow(\theta = \pi/2)\mathbf{e}_y$ , gives rise to a periodic modulation of the spin-resolved electronic charge density, written as

$$\rho_s(\mathbf{r}) = \rho_s(\mathbf{Q}_s^{\text{op}}) e^{i\mathbf{Q}_s^{\text{op}} \cdot \mathbf{r}} + \text{c.c.} = \sum_{\mathbf{k}} \langle c_{\mathbf{k}+\mathbf{Q}_s^{\text{op}},s}^\dagger c_{\mathbf{k}s} \rangle e^{i\mathbf{Q}_s^{\text{op}} \cdot \mathbf{r}} + \text{c.c.} = 2V^{-1} \Delta_s e^{i\mathbf{Q}_s^{\text{op}} \cdot \mathbf{r}} + \text{c.c.} = 4V^{-1} |\Delta_s| \cos(\mathbf{Q}_s^{\text{op}} \cdot \mathbf{r} + \phi_s). \quad (7)$$

Here, the complex order parameter is written as  $\Delta_s = |\Delta_s| e^{i\phi_s}$ , with  $\phi_s$  the corresponding phase [the sliding (translational) phase]. Consequently, our many-body microscopic calculations demonstrate that the ordering wave vectors for spin-up and spin-down electrons condense along two mutually orthogonal directions, forming unique spin-resolved stripe phases that are mutually orthogonal, as shown in Fig. 2(c) and (d).

As a direct consequence of this composite ordered state, the superposition of the two mutually orthogonal spin-resolved stripe orders naturally yields a checkerboard CDW pattern,  $\rho_{\uparrow}(\mathbf{r}) + \rho_{\downarrow}(\mathbf{r})$ , in the charge channel, as shown in Fig. 2(e). In contrast, the spin channel exhibits an antiphase SDW modulation,  $\rho_{\uparrow}(\mathbf{r}) - \rho_{\downarrow}(\mathbf{r})$ , as shown in Fig. 2(f). Such an antiphase SDW modulation of originally itinerant electrons, arising from the incommensurate nature of the density modulation selected by Fermi-surface nesting, is generically accompanied by continuous spatial variations of the internal hyperfine field. Accordingly, the resulting NMR line shape is expected to exhibit a broad and continuous spectrum, rather than a collection of discrete resonance lines. This behavior is fully consistent with NMR experimental observations [32], where a broad and continuous distribution of resonance frequencies develops around the original central frequency upon cooling below 100 K.

Substituting the optimal ordering wave vector  $\mathbf{Q}_s^{\text{op}}$  for each spin sector together with the corresponding gap magnitude  $|\Delta_s|$  into the quasiparticle spectrum [Eq. (5)], clear gap openings emerge near the Fermi level, accompanied by additional bands arising from the particle-hole mixing, as shown in Fig. 2(b). The spin-up sector exhibits a gap along  $\Gamma$ -X direction and the spin-down sector shows gap openings along  $\Gamma$ -Y and X-M, while a spin-degenerate gap opening is observed along  $\Gamma$ -M. These results, obtained without additionally introducing external explicit symmetry breaking (as discussed in Discussion), are in good agreement with low-temperature ARPES measurements [32], which report gap-opening features and additional band reconstructions along  $\Gamma$ -X/Y and Y/X-M directions.

*Phase transitions.*—The finite-temperature behavior and the associated phase transitions require a treatment beyond mean-

field theory, as thermal phase fluctuations of the order parameter in low-dimensional electronic systems become increasingly important at  $T > 0$ . In systems where the phase transition is driven purely by electron–electron interactions, the amplitude of the order parameter remains well captured by the mean-field solution [41, 48–50] whereas the phase degree of freedom must be treated by adopting a bosonized description of the collective phase mode (Nambu–Goldstone boson [51–54], i.e., phason).

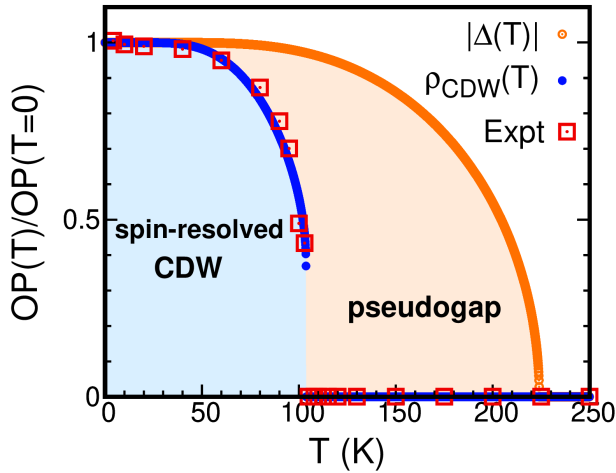


FIG. 3. Temperature dependence of the spin-resolved density-wave modulation amplitude  $\rho_{\text{CDW}}(T) = 4V^{-1}|\Delta_s(T)| \exp(-\langle\delta\phi_s^2(T)\rangle/2)$  and the gap magnitude  $|\Delta(T)| = |\Delta_s(T)|$ . All physical quantities are normalized by their respective  $T = 0$  values, showing the thermal evolution of experimentally accessible observables upon heating and across the phase transitions. Experimental data are taken from Ref. [32] and extracted from the temperature dependence of the spectral splitting observed in NMR measurements, assuming that the splitting is proportional to the spin-resolved density order  $\rho_{\text{CDW}}$ . Specific parameters used in our calculation are presented in Sec. SIV.

We decompose the phase as  $\phi_s = \phi_s^e + \delta\phi_s$  where  $\delta\phi_s$  denotes phase fluctuations around equilibrium configuration  $\phi_s^e$ , and hence, the average of density-wave order reads (Sec. SIII)

$$\langle\rho_s(\mathbf{r})\rangle = 4V^{-1}|\Delta_s|\langle\cos(\mathbf{Q}_s^{\text{op}} \cdot \mathbf{r} + \phi_s)\rangle = 4V^{-1}|\Delta_s|\exp(-\langle\delta\phi_s^2\rangle/2)\cos(\mathbf{Q}_s^{\text{op}} \cdot \mathbf{r} + \phi_s^e), \quad (8)$$

in which a Debye–Waller-like factor [55, 56]  $\exp(-\langle\delta\phi_s^2\rangle/2)$  emerges from phase fluctuations (Sec. SIII A). Then, the temperature dependence of the density-wave order and the phase transitions are governed not only by the gap, but also by thermal phase fluctuations. This separation naturally accounts for the suppression of long-range coherence at finite temperatures, even in the presence of a robust single-particle gap. The average of phase fluctuations takes a generalized form [48, 57–60] (see Sec. SIII C for detailed microscopic derivation),

$$\langle\delta\phi_s^2\rangle/2 = \int \frac{d\mathbf{q}}{(2\pi)^2} \frac{2n_B(\Omega_s(\mathbf{q})) + 1}{D_s\Omega_s(\mathbf{q})}, \quad (9)$$

where  $D_s$  is the phason inertia (temporal stiffness, see Sec. SI),  $n_B(x)$  is the Bose–Einstein distribution, and the energy spectrum of the bosonic phason  $\Omega_s(\mathbf{q})$  is the dispersion of the

bosonic phason mode, given by (see Sec. SIII B)

$$\Omega_s^2(\mathbf{q}) = m_p^2(T) + f_c(T)(\mathbf{v}_s \cdot \mathbf{q})^2, \quad (10)$$

where  $f_c(T)$  is the condensation fraction expressed as a function of  $|\Delta|$  (see Sec. SI),  $\mathbf{v}_s$  is the phason velocity, and  $m_p$  represents the excitation gap of the phason, which originates from the pinning of the density-wave order due to impurities [61], commensurability effect or lattice imperfections [37, 38]. The pinning strength obeys a self-consistent temperature dependence  $m_p^2(T) = m_p^2(0) \exp(-\langle\delta\phi_s^2(T)\rangle/2)|\Delta(T)|/|\Delta(0)|$  (see Sec. SIII B), which reflects the feedback between thermal phase fluctuations and the effective pinning and describes the phason softening as temperature increases. When the phason softens and becomes nearly gapless upon approaching the critical temperature, the absence of an excitation gap removes infrared protection, leading to divergent phase fluctuations in accordance with the Mermin–Wagner theorem [62–64]. Then, the density-wave order is expected to be rapidly suppressed in the vicinity of this transition (see Sec. SV for detailed discussion).

Solving self-consistently the gap equation [Eq. (6)] and fluctuation equation [Eqs. (9) and (10)] as well as  $f_c(T)$  in Eq. (S) leads to the finite-temperature phase evolution and phase transitions shown in Fig. 3. As the temperature increases, the progressively enhanced thermal phase fluctuations lead to a rapid suppression of the density-wave order  $\rho_{\text{CDW}}(T)$ , while the gap amplitude  $|\Delta(T)|$  exhibits a relatively slow decrease with temperature. The former behavior is governed by bosonic thermal fluctuations, whereas the latter is primarily controlled by the thermal occupation of fermionic quasiparticles. Thus, the disappearance of the density-wave ordered state at finite temperatures is controlled by the divergence of thermal phase fluctuations as the phason softens toward a nearly gapless mode, rather than by a collapse of the mean-field gap amplitude. This provides a natural mechanism for a phase-disordered yet gapped state (a pseudogap regime) above the transition temperature. As a result, as seen from Fig. 3, the density-wave order  $\rho_{\text{CDW}}(T)$  melts at  $T_c \approx 100$  K, with a pronounced and rapid suppression in the vicinity of  $T_c$ , whereas the gap opening  $|\Delta(T)|$  persists, giving rise to a robust pseudogap regime, which eventually closes at a higher temperature  $T_g \approx 225$  K. These features, including the temperature dependence of density-wave order  $\rho_{\text{CDW}}(T)$  as well as the values of  $T_c$  and  $T_g$  exhibit quantitative agreement with the experimental observations [32], where NMR signatures of the density-wave order vanish above 100 K, while the single-particle gap observed in ARPES remains finite up to temperatures of  $\sim 230$  K.

*Discussion.*—Regarding other possibilities of ground state, previous DFT studies [32, 34, 36] supporting an SDW interpretation typically start by assuming a specific ordering vector  $\mathbf{Q}_0 = (\pi/a, \pi/a)$  to construct an enlarged magnetic unit cell. Gap opening in the electronic spectrum in these studies is then achieved by explicitly breaking additional symmetries, for example by prescribing particular spin configurations or by introducing enhanced on-site correlation effects on selected magnetic sites. Such a treatment is closer to a band reconstruction caused by an externally imposed magnetic ordering pat-

tern in an enlarged unit cell that reshapes the electronic bands via Brillouin-zone folding and additional external symmetry breaking rather than to a genuine itinerant SDW instability arising self-consistently from electronic condensation.

As shown in Fig. 2(a), there exists essentially no angular window in which both  $|\Delta_{\mathbf{Q}_\uparrow}(\theta_{\mathbf{Q}_\uparrow})|$  and  $|\Delta_{\mathbf{Q}_\downarrow}(\theta_{\mathbf{Q}_\downarrow})|$  remain finite simultaneously. This indicates that the spin-up and spin-down electrons are energetically disfavored to condense at the same ordering wave vector. Theoretically, quasi-1D systems tend to favor nesting driven by their own Fermi-surface geometry, and a single ordering wave vector cannot efficiently connect two orthogonal quasi-1D Fermi-surface segments without severely restricting the available phase space for pairing (see Sec. SVII). As a result, an electronic SDW state modulated at single  $\mathbf{Q}$ , involving both spin sectors without an accompanying charge modulation, is not generically expected in this case.

Through a self-consistent microscopic many-body calculation, the present study provides an alternative interpretation in terms of a spin-resolved electronic CDW instability, consisting of mutually orthogonal stripe modulations in the spin-up and spin-down sectors. The resulting simulations naturally account for the key experimental observations from ARPES and NMR [32], including pronounced gap openings near the Fermi surface (obtained without additionally introducing external explicit symmetry breaking), an electronic antiphase-SDW modulation (consistent with a broad and continuous NMR spectral profile), and an extended pseudogap regime driven by thermal phase fluctuations (a hallmark of electronic condensation). We thus call for targeted experimental probes to test the proposed scenario, in particular through detection of the emergent checkerboard CDW order in the charge channel, using real-space or momentum-resolved techniques. More broadly, the proposed composite spin-resolved CDW order arises intrinsically from the spin-dependent topology of the altermagnetic bands, and therefore constitutes a distinctive class of electronic instability unique to metallic altermagnets with strong  $d$ -wave spin-momentum locking, extending well beyond the specific material  $KV_2Se_2O$  studied here. Notably, the extended pseudogap phenomena identified here and the associated tractable fully microscopic framework we develop are general and applicable to a broad class of low-dimensional CDW materials beyond the specific context of altermagnetic systems.

*Acknowledgments.*—This work is supported by the US Department of Energy, Office of Science, Basic Energy Sciences, under Award Number DE-SC0020145 as part of Computational Materials Sciences Program. F.Y. and L.Q.C. also appreciate the generous support from the Donald W. Hamer Foundation through a Hamer Professorship at Penn State.

031042 (2022).

- [2] L. Šmejkal, J. Sinova, and T. Jungwirth, Emerging research landscape of altermagnetism, *Phys. Rev. X* **12**, 040501 (2022).
- [3] S. Bhowal and N. A. Spaldin, Ferroically ordered magnetic octupoles in  $d$ -wave altermagnets, *Phys. Rev. X* **14**, 011019 (2024).
- [4] H. Reichlová, R. Lopes Seeger, R. González-Hernández, I. Kounta, R. Schlitz, D. Kriegner, P. Ritzinger, M. Lammel, M. Leiviskä, A. Birk Hellenes, K. Olejník, V. Petříček, P. Doležal, L. Horák, E. Schmoranzerová, A. Badura, S. Bertaina, A. Thomas, V. Baltz, L. Michez, J. Sinova, S. T. B. Goennenwein, T. Jungwirth, and L. Šmejkal, Observation of a spontaneous anomalous Hall response in the  $Mn_5Si_3$   $d$ -wave altermagnet candidate, *Nat. Commun.* **15**, 4961 (2024).
- [5] J. Ding, Z. Jiang, X. Chen, Z. Tao, Z. Liu, T. Li, J. Liu, J. Sun, J. Cheng, J. Liu, Y. Yang, R. Zhang, L. Deng, W. Jing, Y. Huang, Y. Shi, M. Ye, S. Qiao, Y. Wang, Y. Guo, D. Feng, and D. Shen, Large band splitting in  $g$ -wave altermagnet CrSb, *Phys. Rev. Lett.* **133**, 206401 (2024).
- [6] Z. Liu, M. Ozeki, S. Asai, S. Itoh, and T. Masuda, Chiral split magnon in altermagnetic MnTe, *Phys. Rev. Lett.* **133**, 156702 (2024).
- [7] F. Zhang, X. Cheng, Z. Yin, C. Liu, L. Deng, Y. Qiao, Z. Shi, S. Zhang, J. Lin, Z. Liu, M. Ye, Y. Huang, X. Meng, C. Zhang, T. Okuda, K. Shimada, S. Cui, Y. Zhao, G.-H. Cao, S. Qiao, J. Liu, and C. Chen, Crystal-symmetry-paired spin-valley locking in a layered room-temperature metallic altermagnet candidate, *Nat. Phys.* **21**, 760 (2025).
- [8] L. Bai, W. Feng, S. Liu, L. Šmejkal, Y. Mokrousov, and Y. Yao, Altermagnetism: Exploring new frontiers in magnetism and spintronics, *Adv. Funct. Mater.* **34**, 2409327.
- [9] M. Weißenhofer and A. Marmodoro, Atomistic spin dynamics simulations of magnonic spin seebeck and spin nernst effects in altermagnets, *Phys. Rev. B* **110**, 094427 (2024).
- [10] R. González-Hernández, L. Šmejkal, K. Výborný, Y. Yahagi, J. Sinova, T. c. v. Jungwirth, and J. Železný, Efficient electrical spin splitter based on nonrelativistic collinear antiferromagnetism, *Phys. Rev. Lett.* **126**, 127701 (2021).
- [11] H. Bai, Y. C. Zhang, Y. J. Zhou, P. Chen, C. H. Wan, L. Han, W. X. Zhu, S. X. Liang, Y. C. Su, X. F. Han, F. Pan, and C. Song, Efficient spin-to-charge conversion via altermagnetic spin splitting effect in antiferromagnet  $RuO_2$ , *Phys. Rev. Lett.* **130**, 216701 (2023).
- [12] Y. J. Sun, F. Yang, and L. Q. Chen, Spin relaxation and transport behavior in  $d$ -wave altermagnetic systems, *Phys. Rev. B* **112**, 024412 (2025).
- [13] T. Jungwirth, J. Sinova, P. Wadley, D. Kriegner, H. Reichlova, F. Krizek, H. Ohno, and L. Smejkal, Altermagnetic spintronics, arXiv:2508.09748 (2025).
- [14] Z. Feng, X. Zhou, L. Šmejkal, L. Wu, Z. Zhu, H. Guo, R. González-Hernández, X. Wang, H. Yan, P. Qin, X. Zhang, H. Wu, H. Chen, Z. Meng, L. Liu, Z. Xia, J. Sinova, T. Jungwirth, and Z. Liu, An anomalous Hall effect in altermagnetic ruthenium dioxide, *Nat. Electron.* **5**, 735 (2022).
- [15] C.-T. Liao, Y.-C. Wang, Y.-C. Tien, S.-Y. Huang, and D. Qu, Separation of inverse altermagnetic spin-splitting effect from inverse spin hall effect in  $RuO_2$ , *Phys. Rev. Lett.* **133**, 056701 (2024).
- [16] T. Sato, S. Haddad, I. C. Fulga, F. F. Assaad, and J. van den Brink, Altermagnetic anomalous hall effect emerging from electronic correlations, *Phys. Rev. Lett.* **133**, 086503 (2024).
- [17] H.-Y. Ma, M. Hu, N. Li, J. Liu, W. Yao, J.-F. Jia, and J. Liu, Multifunctional antiferromagnetic materials with giant piezomagnetism and noncollinear spin current, *Nat. Commun.* **12**,

\* fzy5099@psu.edu

† lqc3@psu.edu

[1] L. Šmejkal, J. Sinova, and T. Jungwirth, Beyond conventional ferromagnetism and antiferromagnetism: A phase with nonrelativistic spin and crystal rotation symmetry, *Phys. Rev. X* **12**,

2846 (2021).

[18] P.-H. Fu, Q. Lv, Y. Xu, J. Cayao, J.-F. Liu, and X.-L. Yu, All-electrically controlled spintronics in altermagnetic heterostructures, *npj Quantum Mater.* **10**, 111 (2025).

[19] Y. Fukaya, B. Lu, K. Yada, Y. Tanaka, and J. Cayao, Superconducting phenomena in systems with unconventional magnets, arXiv:2502.15400 (2025).

[20] Y. Fukaya, K. Maeda, K. Yada, J. Cayao, Y. Tanaka, and B. Lu, Josephson effect and odd-frequency pairing in superconducting junctions with unconventional magnets, *Phys. Rev. B* **111**, 064502 (2025).

[21] W. Zhao, Y. Fukaya, P. Burset, J. Cayao, Y. Tanaka, and B. Lu, Orientation-dependent transport in junctions formed by  $d$ -wave altermagnets and  $d$ -wave superconductors, *Phys. Rev. B* **111**, 184515 (2025).

[22] J. A. Ouassou, A. Brataas, and J. Linder, dc josephson effect in altermagnets, *Phys. Rev. Lett.* **131**, 076003 (2023).

[23] C. Sun, A. Brataas, and J. Linder, Andreev reflection in altermagnets, *Phys. Rev. B* **108**, 054511 (2023).

[24] Y.-M. Wu, Y. Wang, and R. M. Fernandes, Intra-unit-cell singlet pairing mediated by altermagnetic fluctuations, *Phys. Rev. Lett.* **135**, 156001 (2025).

[25] F. Yang and L. Q. Chen, Altermagnetism-induced noncollinear superconducting diode effect and unidirectional superconducting transport, *Phys. Rev. B* **112**, L220502 (2025).

[26] J. Krempaský, L. Šmejkal, S. W. D’Souza, M. Hajlaoui, G. Springholz, K. Uhlířová, F. Alarab, P. C. Constantinou, V. Stročov, D. Usanov, W. R. Pudelko, R. González-Hernández, A. Birk Hellenes, Z. Jansa, H. Reichlová, Z. Šobáň, R. D. Gonzalez Betancourt, P. Wadley, J. Sinova, D. Kriegner, J. Minár, J. H. Dil, and T. Jungwirth, Altermagnetic lifting of Kramers spin degeneracy, *Nature* **626**, 517 (2024).

[27] T. Osumi, S. Souma, T. Aoyama, K. Yamauchi, A. Honma, K. Nakayama, T. Takahashi, K. Ohgushi, and T. Sato, Observation of a giant band splitting in altermagnetic MnTe, *Phys. Rev. B* **109**, 115102 (2024).

[28] S. Lee, S. Lee, S. Jung, J. Jung, D. Kim, Y. Lee, B. Seok, J. Kim, B. G. Park, L. Šmejkal, C.-J. Kang, and C. Kim, Broken kramers degeneracy in altermagnetic MnTe, *Phys. Rev. Lett.* **132**, 036702 (2024).

[29] Y.-P. Zhu, X. Chen, X.-R. Liu, Y. Liu, P. Liu, H. Zha, G. Qu, C. Hong, J. Li, Z. Jiang, X.-M. Ma, Y.-J. Hao, M.-Y. Zhu, W. Liu, M. Zeng, S. Jayaram, M. Lenger, J. Ding, S. Mo, K. Tanaka, M. Arita, Z. Liu, M. Ye, D. Shen, J. Wrachtrup, Y. Huang, R.-H. He, S. Qiao, Q. Liu, and C. Liu, Observation of plaid-like spin splitting in a noncoplanar antiferromagnet, *Nature* **626**, 523 (2024).

[30] M. Hiraishi, H. Okabe, A. Koda, R. Kadono, T. Muroi, D. Hirai, and Z. Hiroi, Nonmagnetic ground state in RuO<sub>2</sub> revealed by muon spin rotation, *Phys. Rev. Lett.* **132**, 166702 (2024).

[31] P. Keßler, L. Garcia-Gassull, A. Suter, T. Prokscha, Z. Salman, D. Khalyavin, P. Manuel, F. Orlandi, I. I. Mazin, R. Valentí, and S. Moser, Absence of magnetic order in RuO<sub>2</sub>: insights from  $\mu$ sr spectroscopy and neutron diffraction, *npj Spintronics* **2**, 50 (2024).

[32] B. Jiang, M. Hu, J. Bai, Z. Song, C. Mu, G. Qu, W. Li, W. Zhu, H. Pi, Z. Wei, Y.-J. Sun, Y. Huang, X. Zheng, Y. Peng, L. He, S. Li, J. Luo, Z. Li, G. Chen, H. Li, H. Weng, and T. Qian, A metallic room-temperature  $d$ -wave altermagnet, *Nat. Phys.* **21**, 754 (2025).

[33] J. Lai, T. Yu, P. Liu, L. Liu, G. Xing, X.-Q. Chen, and Y. Sun,  $d$ -wave flat fermi surface in altermagnets enables maximum charge-to-spin conversion, *Phys. Rev. Lett.* **135**, 256702 (2025).

[34] Y. Xu, H. Zhang, M. Feng, and F. Tian, Electronic structure, magnetic transition, and fermi surface instability of the room-temperature altermagnet KV<sub>2</sub>Se<sub>2</sub>O, *Phys. Rev. B* **112**, 125141 (2025).

[35] X. Yang, S. Fang, Z. Yang, P. Ho, J. Lu, and Y. S. Ang, Altermagnetic flatband-driven fermi surface geometry for giant tunneling magnetoresistance, arXiv:2511.17277 (2025).

[36] X. Yan, Z. Song, J. Song, Z. Fang, H. Weng, and Q. Wu, Sdw driven “magnetic breakdown” in a  $d$ -wave altermagnet KV<sub>2</sub>Se<sub>2</sub>O, arXiv:2505.00074 (2025).

[37] G. Grüner and A. Zettl, Charge density wave conduction: A novel collective transport phenomenon in solids, *Physics Reports* **119**, 117 (1985).

[38] G. Grüner, The dynamics of charge-density waves, *Rev. Mod. Phys.* **60**, 1129 (1988).

[39] P. Lee, T. Rice, and P. Anderson, Conductivity from charge or spin density waves, *Solid State Communications* **14**, 703 (1974).

[40] R. E. Peierls, *Quantum theory of solids* (Clarendon Press, 1996).

[41] M. Hoyer and J. Schmalian, Role of fluctuations for density-wave instabilities: Failure of the mean-field description, *Phys. Rev. B* **97**, 224423 (2018).

[42] T. M. Rice and G. K. Scott, New mechanism for a charge-density-wave instability, *Phys. Rev. Lett.* **35**, 120 (1975).

[43] X. Huang and K. Maki, Imperfect nesting in quasi-one-dimensional charge- and spin-density waves, *Phys. Rev. B* **42**, 6498 (1990).

[44] G. Kresse and J. Furthmüller, Efficiency of ab-initio total energy calculations for metals and semiconductors using a plane-wave basis set, *Comp. Mater. Sci.* **6**, 15 (1996).

[45] G. Kresse and J. Furthmüller, Efficient iterative schemes for ab initio total-energy calculations using a plane-wave basis set, *Phys. Rev. B* **54**, 11169 (1996).

[46] J. P. Perdew, K. Burke, and M. Ernzerhof, Generalized gradient approximation made simple, *Phys. Rev. Lett.* **77**, 3865 (1996).

[47] L. Šmejkal, A. B. Hellenes, R. González-Hernández, J. Sinova, and T. Jungwirth, Giant and tunneling magnetoresistance in unconventional collinear antiferromagnets with nonrelativistic spin-momentum coupling, *Phys. Rev. X* **12**, 011028 (2022).

[48] F. Yang, G. Zhao, Y. Shi, and L. Chen, An efficient phase-transition framework for gate-tunable superconductivity in monolayer wte  $\mathcal{Z}$ , arXiv:2509.08332 (2025).

[49] i. c. v. Kos, A. J. Millis, and A. I. Larkin, Gaussian fluctuation corrections to the bcs mean-field gap amplitude at zero temperature, *Phys. Rev. B* **70**, 214531 (2004).

[50] S. Fischer, M. Hecker, M. Hoyer, and J. Schmalian, Short-distance breakdown of the higgs mechanism and the robustness of the bcs theory for charged superconductors, *Phys. Rev. B* **97**, 054510 (2018).

[51] Y. Nambu, Quasi-particles and gauge invariance in the theory of superconductivity, *Phys. Rev.* **117**, 648 (1960).

[52] J. Goldstone, Field theories with “superconductor” solutions, *Il Nuovo Cimento* **19**, 154 (1961).

[53] J. Goldstone, A. Salam, and S. Weinberg, Broken symmetries, *Phys. Rev.* **127**, 965 (1962).

[54] Y. Nambu, Nobel lecture: Spontaneous symmetry breaking in particle physics: A case of cross fertilization, *Rev. Mod. Phys.* **81**, 1015 (2009).

[55] C. Kittel and C.-y. Fong, *Quantum theory of solids*, Vol. 5 (Wiley New York, 1963).

[56] J. J. Sakurai and J. Napolitano, *Modern quantum mechanics* (Cambridge University Press, 2020).

[57] F. Yang and L. Chen, Microscopic phase-transition theory of charge density waves: revealing hidden transitions of phason and amplitudon, arXiv:2505.05025 (2025).

[58] F. Yang, Y. Shi, and L.-Q. Chen, Preformed cooper pairing and

the uncondensed normal-state component in phase-fluctuating cuprate superconductivity, arXiv:2509.21133 (2025).

[59] F. Yang and L. Chen, A tractable framework for phase transitions in phase-fluctuating disordered 2D superconductors: applications to bilayer  $\text{MoS}_2$  and disordered  $\text{InO}_x$  thin films, arXiv preprint arXiv:2511.13268 (2025).

[60] T. M. Rice, S. Whitehouse, and P. Littlewood, Impurity pinning of discommensurations in charge-density waves, *Phys. Rev. B* **24**, 2751 (1981).

[61] H. Fukuyama and P. A. Lee, Dynamics of the charge-density wave. I. impurity pinning in a single chain, *Phys. Rev. B* **17**, 535 (1978).

[62] P. C. Hohenberg, Existence of long-range order in one and two dimensions, *Phys. Rev.* **158**, 383 (1967).

[63] N. D. Mermin and H. Wagner, Absence of ferromagnetism or antiferromagnetism in one- or two-dimensional isotropic heisenberg models, *Phys. Rev. Lett.* **17**, 1133 (1966).

[64] S. Coleman, There are no goldstone bosons in two dimensions, *Commun. Math. Phys.* **31**, 259 (1973).

# Emergent spin-resolved electronic charge density waves and pseudogap phenomena from strong *d*-wave altermagnetism (Supplemental Materials)

Fei Yang,<sup>1,\*</sup> Guo-Dong Zhao,<sup>1</sup> Binghai Yan,<sup>2</sup> and Long-Qing Chen<sup>1,†</sup>

<sup>1</sup>*Department of Materials Science and Engineering and Materials Research Institute,  
The Pennsylvania State University, University Park, PA 16802, USA*

<sup>2</sup>*Department of Physics, The Pennsylvania State University, University Park, PA 16802, USA*

## SI. Derivation of the effective action

In this section, we present a microscopic derivation of the low-energy effective action starting from a fermionic Hamiltonian with the effective spin-conserving electron-electron interactions (extended Hubbard interactions). By integrating out the fermionic degrees of freedom, we obtain a controlled description of the density-wave order parameter and its associated collective fluctuations in the ordered state. For notational simplicity, throughout the derivation we focus on a single spin sector and suppress the explicit spin index. This choice does not entail any loss of generality, since different spin components are decoupled in the context of the spin-resolved CDWs considered here.

Based on the Hamiltonian presented in the main text, the action of the model is given by

$$S = \int dx \psi^\dagger(x) (i\partial_t - \xi \hat{\mathbf{p}}) \psi(x) - \int dx dx' \frac{1}{2} U(x - x') \psi^\dagger(x) \psi(x) \psi^\dagger(x') \psi(x'), \quad (\text{S1})$$

where  $\psi(x)$  is the electron field operator,  $\hat{\mathbf{p}} = -i\hbar \nabla$  is the momentum operator, and  $x = (t, \mathbf{x})$  is the space-time four-vector.

We consider an electronic density-wave order condensing at wave vector  $\mathbf{Q}$ , for which the expectation value of the electronic density takes the form [1]

$$\langle \psi^\dagger(x) \psi(x) \rangle = \rho_{\mathbf{Q}}(R) e^{i\mathbf{Q} \cdot \mathbf{x}} + \rho_{-\mathbf{Q}}(R) e^{-i\mathbf{Q} \cdot \mathbf{x}} \quad (\text{S2})$$

where  $R = (t, \mathbf{R})$  denotes a slowly varying (long-wavelength) center-of-mass space-time four-vector [2–5]. Reality of the density field implies  $\rho_{-\mathbf{Q}}(R) = \rho_{\mathbf{Q}}^*(R)$ . Applying a mean-field decoupling in the density-wave channel [6, 7], the action becomes

$$S = \int dx \psi^\dagger(x) [(i\partial_t - \xi \hat{\mathbf{p}}) \psi(x) - U(\mathbf{Q}) \rho_{\mathbf{Q}}(R) \psi^\dagger(x) \psi(x) e^{i\mathbf{Q} \cdot \mathbf{x}} - U(\mathbf{Q}) \rho_{\mathbf{Q}}^*(R) \psi^\dagger(x) \psi(x) e^{-i\mathbf{Q} \cdot \mathbf{x}}] + \int dR U(\mathbf{Q}) |\rho_{\mathbf{Q}}(R)|^2, \quad (\text{S3})$$

Taking  $U(\mathbf{Q}) = V/4$  and defining the order parameter as

$$\Delta_{\mathbf{Q}}(R) = \frac{V}{2} \rho_{\mathbf{Q}}(R), \quad \Delta_{\mathbf{Q}}^*(R) = \frac{V}{2} \rho_{\mathbf{Q}}^*(R), \quad (\text{S4})$$

the action can be written in Nambu space as

$$S = \int dR \left[ \sum_{\mathbf{k}} \frac{1}{2} (\psi_{\mathbf{k}}^\dagger(R), \psi_{\mathbf{k}+\mathbf{Q}}^\dagger(R)) \begin{pmatrix} i\partial_t - \xi_{\mathbf{k}-i\hbar\partial_R} & -\Delta_{\mathbf{Q}}(R) \\ -\Delta_{\mathbf{Q}}^*(R) & i\partial_t - \xi_{\mathbf{k}+\mathbf{Q}-i\hbar\partial_R} \end{pmatrix} \begin{pmatrix} \psi_{\mathbf{k}}(R) \\ \psi_{\mathbf{k}+\mathbf{Q}}(R) \end{pmatrix} + \frac{|\Delta_{\mathbf{Q}}|^2}{V} \right]. \quad (\text{S5})$$

We then treat the density-wave gap and phase on an equal footing within the standard path-integral framework [3, 5, 8, 9]. For convenience, we set  $\hbar = 1$  here and hereafter. Specifically, a general complex density-wave order parameter can be written as

$$\Delta_{\mathbf{Q}}(R) = |\Delta_{\mathbf{Q}}| \exp[i\phi(R)], \quad (\text{S6})$$

with  $\phi(R) = \phi_e + \delta\phi(R)$ . Here,  $|\Delta_{\mathbf{Q}}|$  and  $\phi_e$  denote the density-wave gap and equilibrium phase configuration, respectively, while  $\delta\phi(R)$  represents phase fluctuations. Moreover, for *complex* electronic order parameter ( $N = 2$ , where  $N$  is the dimensionality of the order parameter), amplitude fluctuations are negligible, as they are exactly canceled by short-range fluctuation terms, as demonstrated in Ref. [1]. This cancellation is consistent with earlier theoretical results for superconductors [10, 11] and other systems with complex order parameters [1], in which neither amplitude fluctuations nor short-range-fluctuations corrections

\* fzy5099@psu.edu

† lqc3@psu.edu

modify the self-consistent order-parameter microscopic equation at the thermodynamic level, and where only long-wavelength phase fluctuations play a role.

Substituting  $\mathbf{k} = \delta\mathbf{k} - \mathbf{Q}/2$ , the action can be rewritten in a symmetric form as

$$S = \int dR \left[ \sum_{\delta\mathbf{k}} \frac{1}{2} (\psi_{\delta\mathbf{k}-\mathbf{Q}/2}^\dagger(R), \psi_{\delta\mathbf{k}+\mathbf{Q}/2}^\dagger(R)) \begin{pmatrix} i\partial_t - \xi_{\delta\mathbf{k}-\mathbf{Q}/2-i\hbar\partial_R} & -\Delta_{\mathbf{Q}}(R) \\ -\Delta_{\mathbf{Q}}^*(R) & i\partial_t - \xi_{\delta\mathbf{k}+\mathbf{Q}/2-i\hbar\partial_R} \end{pmatrix} \begin{pmatrix} \psi_{\delta\mathbf{k}-\mathbf{Q}/2}(R) \\ \psi_{\delta\mathbf{k}+\mathbf{Q}/2}(R) \end{pmatrix} + \frac{|\Delta_{\mathbf{Q}}|^2}{V} \right]. \quad (\text{S7})$$

For an open Fermi surface in each spin sector, the ordering wave vector  $\mathbf{Q}$  naturally connects the two Fermi-surface sheets, such that  $\psi_{\delta\mathbf{k}-\mathbf{Q}/2}$  and  $\psi_{\delta\mathbf{k}+\mathbf{Q}/2}$  correspond to quasiparticles on opposite sheets. We then apply the chiral (gauge) transformations [4, 12]

$$\psi_{\delta\mathbf{k}-\mathbf{Q}/2} \rightarrow \psi_{\delta\mathbf{k}-\mathbf{Q}/2} \exp[i\phi(R)/2], \quad \psi_{\delta\mathbf{k}+\mathbf{Q}/2} \rightarrow \psi_{\delta\mathbf{k}+\mathbf{Q}/2} \exp[-i\phi(R)/2], \quad (\text{S8})$$

and neglect trivial total-derivative terms. The action becomes

$$\begin{aligned} S &= \int dR \left\{ \frac{1}{2} \sum_{\delta\mathbf{k}} \Psi_{\delta\mathbf{k}}^\dagger(R) \left[ i\partial_t - \delta\xi_{\delta\mathbf{k}} - \bar{\xi}_{\delta\mathbf{k}}\tau_3 - |\Delta_{\mathbf{Q}}|\tau_1 - \frac{\partial_t\delta\phi}{2}\tau_3 + \frac{\mathbf{v}_{\mathbf{Q}/2} \cdot \partial_{\mathbf{R}}\delta\phi}{2} - \frac{(\partial_{\mathbf{R}}\phi \cdot \mathbf{m}_{\mathbf{Q}/2}^{-1} \cdot \partial_{\mathbf{R}}\phi)}{8} \right] \Psi_{\delta\mathbf{k}}(R) + \frac{|\Delta_{\mathbf{Q}}|^2}{V} \right\} \\ &= \int dR \left[ \frac{1}{2} \sum_{\delta\mathbf{k}} \Psi_{\delta\mathbf{k}}^\dagger(R) (G_0^{-1} - \Sigma) \Psi_{\delta\mathbf{k}}(R) + \frac{|\Delta_{\mathbf{Q}}|^2}{V} \right], \end{aligned} \quad (\text{S9})$$

where  $\tau_i$  denotes the Pauli matrices in Nambu space and Nambu spinor  $\Psi_{\delta\mathbf{k}}^\dagger(R) = (\psi_{\delta\mathbf{k}-\mathbf{Q}/2}^\dagger(R), \psi_{\delta\mathbf{k}+\mathbf{Q}/2}^\dagger(R))$ ; the Green function is determined by

$$G_0^{-1} = i\partial_t - \delta\xi_{\delta\mathbf{k}} - \bar{\xi}_{\delta\mathbf{k}}\tau_3 - |\Delta_{\mathbf{Q}}|\tau_1, \quad (\text{S10})$$

with

$$\delta\xi_{\delta\mathbf{k}} = (\xi_{\delta\mathbf{k}-\mathbf{Q}/2} + \xi_{\delta\mathbf{k}+\mathbf{Q}/2})/2, \quad \bar{\xi}_{\delta\mathbf{k}} = (\xi_{\delta\mathbf{k}-\mathbf{Q}/2} - \xi_{\delta\mathbf{k}+\mathbf{Q}/2})/2, \quad (\text{S11})$$

and the self-energy reads

$$\Sigma = \partial_t\delta\phi/2\tau_3 - \mathbf{v}_{\mathbf{Q}/2} \cdot \partial_{\mathbf{R}}\delta\phi/2 + (\partial_{\mathbf{R}}\phi/2 \cdot \mathbf{m}_{\mathbf{Q}/2}^{-1} \cdot \partial_{\mathbf{R}}\phi/2)/2, \quad (\text{S12})$$

Here,  $\mathbf{v}_{\mathbf{Q}/2} = \partial_{\mathbf{Q}/2}\xi_{\mathbf{Q}/2}$  the group velocity evaluated at momentum, and  $\mathbf{m}_{\mathbf{Q}/2}^{-1} = \partial_{\mathbf{Q}/2}\partial_{\mathbf{Q}/2}\xi_{\mathbf{Q}/2}$  represents the inverse effective-mass tensor. Then, through the standard integration over the Fermi field in the Matsubara representation [6–8], one has

$$S = \int dR \left\{ -\bar{\text{Tr}} \ln G_0^{-1} + \sum_n^\infty \frac{1}{n} \bar{\text{Tr}}[(\Sigma G_0)^n] + \frac{|\Delta_{\mathbf{Q}}|^2}{V} \right\}, \quad (\text{S13})$$

where the Green function in the Matsubara representation:

$$G_0(ip_n, \delta\mathbf{k}) = \frac{ip_n\tau_0 - \delta\xi_{\delta\mathbf{k}}\tau_0 + \bar{\xi}_{\delta\mathbf{k}}\tau_3 + |\Delta_{\mathbf{Q}}|\tau_1}{(ip_n - E_{\delta\mathbf{k}}^+)(ip_n - E_{\delta\mathbf{k}}^-)}, \quad (\text{S14})$$

with

$$E_{\delta\mathbf{k}}^\pm = \delta\xi_{\delta\mathbf{k}} \pm E_{\delta\mathbf{k}}, \quad E_{\delta\mathbf{k}} = \sqrt{\bar{\xi}_{\delta\mathbf{k}}^2 + |\Delta_{\mathbf{Q}}|^2}. \quad (\text{S15})$$

Further keeping the lowest two orders (i.e.,  $n = 1$  and  $n = 2$ ) and neglecting the trivial terms lead to the result:

$$S_{\text{eff}} = \int dR \left[ -\frac{1}{2} \sum_{ip_n, \delta\mathbf{k}} \ln[(ip_n - E_k^+)(ip_n - E_k^-)] + \frac{|\Delta_{\mathbf{Q}}|^2}{V} + \chi_{33} \left( \frac{\partial_t\delta\phi}{2} \right)^2 + \chi_{00} \left( \frac{\mathbf{v}_{\mathbf{Q}/2} \cdot \partial_{\mathbf{R}}\delta\phi}{2} \right)^2 + \chi_0 \frac{(\partial_{\mathbf{R}}\phi \cdot \mathbf{m}_{\mathbf{Q}/2}^{-1} \cdot \partial_{\mathbf{R}}\phi)}{8} \right] \quad (\text{S16})$$

Here, the correlation coefficients related to the phase sector are given by

$$\chi_0 = \frac{1}{2} \sum_{ip_n, \delta\mathbf{k}} \text{Tr}[G_0(ip_n, \delta\mathbf{k})] = \frac{1}{2} \sum_{\delta\mathbf{k}} [f(E_{\delta\mathbf{k}}^+) + f(E_{\delta\mathbf{k}}^-)], \quad (\text{S17})$$

$$\begin{aligned} \chi_{33} &= \frac{1}{4} \sum_{ip_n, \delta\mathbf{k}} \text{Tr}[G_0(ip_n, \delta\mathbf{k})\tau_3 G_0(ip_n, \delta\mathbf{k})\tau_3] = \frac{1}{2} \sum_{ip_n, \delta\mathbf{k}} \frac{(ip_n - \delta\xi_{\delta\mathbf{k}})^2 + \bar{\xi}_{\delta\mathbf{k}}^2 - |\Delta_{\mathbf{Q}}|^2}{[(ip_n - \delta\xi_{\delta\mathbf{k}})^2 - \bar{\xi}_{\delta\mathbf{k}}^2 - |\Delta_{\mathbf{Q}}|^2]^2} \\ &= \frac{1}{2} \sum_{ip_n, \delta\mathbf{k}} \partial_{\bar{\xi}_{\delta\mathbf{k}}} \left[ \frac{\bar{\xi}_{\delta\mathbf{k}}}{(ip_n - E_{\delta\mathbf{k}}^+)(ip_n - E_{\delta\mathbf{k}}^-)} \right] = \frac{1}{2} \sum_{\delta\mathbf{k}} \partial_{\bar{\xi}_{\delta\mathbf{k}}} \left[ \bar{\xi}_{\delta\mathbf{k}} \frac{f(E_{\delta\mathbf{k}}^+) - f(E_{\delta\mathbf{k}}^-)}{2E_{\delta\mathbf{k}}} \right] = -D, \end{aligned} \quad (\text{S18})$$

$$\begin{aligned} \chi_{00} &= \frac{1}{4} \sum_{ip_n, \delta\mathbf{k}} \text{Tr}[G_0(ip_n, \delta\mathbf{k})G_0(ip_n, \delta\mathbf{k})] = \frac{1}{2} \sum_{ip_n, \delta\mathbf{k}} \frac{(i - \delta\xi_{\delta\mathbf{k}})^2 + \bar{\xi}_{\delta\mathbf{k}}^2 + |\Delta_{\mathbf{Q}}|^2}{[(i - \delta\xi_{\delta\mathbf{k}})^2 - \bar{\xi}_{\delta\mathbf{k}}^2 - |\Delta_{\mathbf{Q}}|^2]^2} \\ &= \frac{1}{2} \sum_{\delta\mathbf{k}} \partial_{E_{\delta\mathbf{k}}} \left[ \frac{f(E_{\delta\mathbf{k}}^+) - f(E_{\delta\mathbf{k}}^-)}{2} \right] = \frac{1}{2} \sum_{\delta\mathbf{k}} \frac{|\Delta_{\mathbf{Q}}|^2}{E_{\delta\mathbf{k}}} \partial_{E_{\delta\mathbf{k}}} \left[ \frac{f(E_{\delta\mathbf{k}}^+) - f(E_{\delta\mathbf{k}}^-)}{2E_{\delta\mathbf{k}}} \right] + \frac{1}{2} \sum_{\delta\mathbf{k}} \partial_{\bar{\xi}_{\delta\mathbf{k}}} \left[ \bar{\xi}_{\delta\mathbf{k}} \frac{f(E_{\delta\mathbf{k}}^+) - f(E_{\delta\mathbf{k}}^-)}{2E_{\delta\mathbf{k}}} \right]. \end{aligned} \quad (\text{S19})$$

Mathematically, by decomposing  $\delta\mathbf{k} = \delta k_{\parallel} \hat{\mathbf{Q}} + \delta\mathbf{k}_{\perp}$  with  $\delta k_{\parallel} \equiv \delta\mathbf{k} \cdot \hat{\mathbf{Q}}$ , and linearizing the nested bands within a low-energy patch,  $\bar{\xi}_{\delta\mathbf{k}} \simeq v_{\parallel} \delta k_{\parallel}$  with  $v_{\parallel} \equiv \mathbf{v}_{\mathbf{Q}/2} \cdot \hat{\mathbf{Q}}$ , one has  $\partial_{\bar{\xi}_{\delta\mathbf{k}}} = (1/v_{\parallel}) \partial_{\delta k_{\parallel}}$ . Then one obtains

$$\begin{aligned} &\mathbf{v}_{\mathbf{Q}/2} \mathbf{v}_{\mathbf{Q}/2} \frac{1}{2} \sum_{\delta\mathbf{k}} \partial_{\bar{\xi}_{\delta\mathbf{k}}} \left[ \bar{\xi}_{\delta\mathbf{k}} \frac{f(E_{\delta\mathbf{k}}^+) - f(E_{\delta\mathbf{k}}^-)}{2E_{\delta\mathbf{k}}} \right] + \frac{\mathbf{m}_{\mathbf{Q}/2}^{-1}}{2} \frac{1}{2} \sum_{\delta\mathbf{k}} [f(E_{\delta\mathbf{k}}^+) + f(E_{\delta\mathbf{k}}^-)] \\ &= \frac{1}{2} \int d\delta k_{\perp} \int_{-\Lambda_{\parallel}}^{\Lambda_{\parallel}} d\delta k_{\parallel} \frac{\mathbf{v}_{\mathbf{Q}/2} \mathbf{v}_{\mathbf{Q}/2}}{v_{\parallel}} \partial_{\delta k_{\parallel}} \left[ \bar{\xi}_{\delta\mathbf{k}} \frac{f(E_{\delta\mathbf{k}}^+) - f(E_{\delta\mathbf{k}}^-)}{2E_{\delta\mathbf{k}}} \right] + \frac{1}{2} \int d\delta k_{\perp} \int_{-\Lambda_{\parallel}}^{\Lambda_{\parallel}} d\delta k_{\parallel} \frac{\mathbf{m}_{\mathbf{Q}/2}^{-1}}{2} \frac{f(E_{\delta\mathbf{k}}^+) + f(E_{\delta\mathbf{k}}^-)}{2} \\ &= \frac{1}{2} \int d\delta k_{\perp} \left\{ \frac{\mathbf{v}_{\mathbf{Q}/2} \mathbf{v}_{\mathbf{Q}/2}}{v_{\parallel}} \left[ \bar{\xi}_{\delta\mathbf{k}} \frac{f(E_{\delta\mathbf{k}}^+) - f(E_{\delta\mathbf{k}}^-)}{2E_{\delta\mathbf{k}}} \right]_{-\Lambda_{\parallel}}^{+\Lambda_{\parallel}} + \int_{-\Lambda_{\parallel}}^{\Lambda_{\parallel}} d\delta k_{\parallel} \frac{\mathbf{m}_{\mathbf{Q}/2}^{-1}}{2} \frac{f(E_{\delta\mathbf{k}}^+) + f(E_{\delta\mathbf{k}}^-)}{2} \right\}. \end{aligned} \quad (\text{S20})$$

The above combination is constrained by the Ward identity associated with translational invariance (equivalently, charge conservation in the chiral basis) [13], i.e., the density-wave analog of the paramagnetic–diamagnetic cancellation in the longitudinal response [8]. After subtracting the normal-state contribution, the boundary term vanishes at  $|\bar{\xi}| \sim \Lambda_E \equiv v_{\parallel} \Lambda_{\parallel}$  and exactly cancels the diamagnetic piece in the perfectly nested and linearized limit. Away from this limit, the residual is controlled by particle–hole asymmetry and imperfect nesting, and is parametrically small, scaling as  $\mathcal{O}(|\Delta_{\mathbf{Q}}|^2/\Lambda_E^2) \sim \mathcal{O}(|\Delta_{\mathbf{Q}}|^2/E_F^2)$ .

Consequently, the final result is written as

$$S_{\text{eff}} = S_{\text{gap}} + S_{\text{phase}}, \quad (\text{S21})$$

with the gap-related part

$$S_{\text{gap}} = \int dR \left[ -\frac{1}{2} \sum_{ip_n, \delta\mathbf{k}} \ln[(ip_n - E_k^+)(ip_n - E_k^-)] + \frac{|\Delta_{\mathbf{Q}}|^2}{V} \right], \quad (\text{S22})$$

and the phase-related one

$$S_{\text{phase}} = \int dR \left[ -D \left( \frac{\partial_t \delta\phi}{2} \right)^2 + D f_c \left( \frac{\mathbf{v}_{\mathbf{Q}/2} \cdot \partial_{\mathbf{R}} \delta\phi}{2} \right)^2 \right], \quad (\text{S23})$$

where temporal stiffness  $D$  is given by

$$D = -\frac{1}{2} \sum_{\delta\mathbf{k}} \partial_{\bar{\xi}_{\delta\mathbf{k}}} \left[ \bar{\xi}_{\delta\mathbf{k}} \frac{f(E_{\delta\mathbf{k}}^+) - f(E_{\delta\mathbf{k}}^-)}{2E_{\delta\mathbf{k}}} \right], \quad (\text{S24})$$

and the condensation fraction  $f_c$  [2, 14, 15] is determined by

$$f_c = \frac{1}{2D} \sum_{\delta\mathbf{k}} \frac{|\Delta_{\mathbf{Q}}|^2}{E_{\delta\mathbf{k}}} \partial_{E_{\delta\mathbf{k}}} \left[ \frac{f(E_{\delta\mathbf{k}}^+) - f(E_{\delta\mathbf{k}}^-)}{2E_{\delta\mathbf{k}}} \right]. \quad (\text{S25})$$

## SII. Derivation of gap equation

In this section, we derive the self-consistent density-wave gap equation. Starting from Eq. (S21), we impose the equilibrium condition by minimizing the effective action with respect to the density-wave order parameter, i.e.,  $\partial_{|\Delta\mathbf{Q}|} S_{\text{gap}} = 0$ . This yields

$$\frac{1}{2} \sum_{ip_n, \delta\mathbf{k}} \frac{2|\Delta\mathbf{Q}|}{(ip_n - E_k^+)(ip_n - E_k^-)} + \frac{2|\Delta\mathbf{Q}|}{V} = 0 \quad \Rightarrow \quad \frac{1}{V} = -\frac{1}{2} \sum_{ip_n, \delta\mathbf{k}} \frac{1}{(ip_n - E_k^+)(ip_n - E_k^-)} = \frac{1}{2} \sum_{\delta\mathbf{k}} \frac{f(E_{\delta\mathbf{k}}^-) - f(E_{\delta\mathbf{k}}^+)}{2E_{\delta\mathbf{k}}}, \quad (\text{S26})$$

where  $f(x)$  is the Fermi–Dirac distribution function and the quasiparticle excitation spectrum is written as

$$E_{\delta\mathbf{k}}^\pm = (\xi_{\delta\mathbf{k}-\mathbf{Q}/2} + \xi_{\delta\mathbf{k}+\mathbf{Q}/2})/2 \pm E_{\delta\mathbf{k}}, \quad E_{\delta\mathbf{k}} = \sqrt{[(\xi_{\delta\mathbf{k}-\mathbf{Q}/2} - \xi_{\delta\mathbf{k}+\mathbf{Q}/2})/2]^2 + |\Delta\mathbf{Q}|^2}. \quad (\text{S27})$$

By shifting the momentum variable according to  $\mathbf{k} = \delta\mathbf{k} - \mathbf{Q}/2$ , the gap equation presented in the main text is recovered.

We note that in deriving the self-consistent gap equation above, phase fluctuations are not explicitly incorporated into the fermionic spectrum, i.e., the Doppler-shift effect ( $\partial_{|\Delta\mathbf{Q}|} S_{\text{phase}}$ ) associated with phase-induced momentum shifts [3, 4, 16–18] is neglected. This approximation should be regarded as a controlled heuristic approximation for electronic-density-wave systems with a large phase-mode velocity, as commonly adopted in the existing literature. This is because with a large phase-mode velocity, the phase space available for the thermal average of Doppler-shift effects  $\langle(\partial\mathbf{R}\delta\phi/2)^2\rangle \sim \langle(q^2\delta\phi_{\mathbf{q}}/2)^2\rangle$  is strongly restricted. As a result, the corresponding corrections from thermal phase fluctuations to the gap equation are parametrically small and do not qualitatively modify the mean-field solution at finite temperature [3, 4, 16–18]. The explicit inclusion of this effect is not the focus of the present study and will be discussed in a future publication. By contrast, such Doppler-shift effects may become non-negligible in lattice-driven density-wave systems, where the phason energy spectrum is strongly renormalized by the ratio  $m/m^*$  [19–21]. This renormalization leads to a substantial suppression of the phason mode velocity, thereby significantly enlarging the phase space available for the thermal averaging of Doppler-shift effects. In this regime, phase fluctuations can strongly feed back into the fermionic sector and modify the self-consistent gap equation beyond the mean-field level [2].

## SIII. Derivation of phase fluctuations

In this section, we derive the contribution of phase fluctuations. We first clarify their physical importance: phase fluctuations play a crucial role in density-wave systems, as they can suppress long-range order through thermal averaging even when the amplitude of the order parameter remains finite.

Specifically, following Eq. (S4) as well as Eq. (S6) with  $\phi(\mathbf{R}) = \phi_e + \delta\phi(\mathbf{R})$ , the charge-density modulation after electronic condensation is written as

$$\rho(\mathbf{R}) = \rho_{\mathbf{Q}} e^{i\mathbf{Q}\cdot\mathbf{R}} + c.c. = 4V^{-1}|\Delta\mathbf{Q}|\cos(\mathbf{Q}\cdot\mathbf{R} + \phi_e + \delta\phi). \quad (\text{S28})$$

Using the statistic average  $\langle\delta\phi\rangle = 0$  and  $\langle\delta\phi^2\rangle \neq 0$ , the thermal average can be evaluated via the cumulant expansion [6, 7, 13],

$$\begin{aligned} \langle\cos(\phi)\rangle &= \text{Re}[e^{i\phi_e}\langle e^{i\delta\phi}\rangle] = \text{Re}\left[e^{i\phi_e}\sum_{n=0}\frac{\langle(i\delta\phi)^{2n}\rangle}{(2n)!}\right] = \text{Re}\left[e^{i\phi_e}\sum_{n=0}\frac{(2n-1)!!(-1)^n\langle\delta\phi^2\rangle^n}{(2n)!}\right] = \text{Re}\left[e^{i\phi_e}\sum_{n=0}\frac{(-1)^n\langle\delta\phi^2\rangle^n}{2^n n!}\right] \\ &= \text{Re}\left[e^{i\phi_e}e^{-\langle\delta\phi^2\rangle/2}\right] = \cos(\phi_e)e^{-\langle\delta\phi^2\rangle/2}. \end{aligned} \quad (\text{S29})$$

As a result, the thermally averaged density-wave order takes the form

$$\langle\rho(\mathbf{R})\rangle = 4V^{-1}|\Delta\mathbf{Q}|\exp(-\langle\delta\phi^2\rangle/2)\cos(\mathbf{Q}\cdot\mathbf{R} + \phi_e), \quad (\text{S30})$$

where a Debye–Waller-like factor [22, 23]  $\exp(-\langle\delta\phi^2\rangle/2)$  naturally emerges from thermal phase fluctuations. Consequently, the temperature dependence of the density-wave order is governed not only by the gap amplitude, but also by thermal phase fluctuations. This separation naturally accounts for the suppression of long-range coherence at finite temperatures, even in the presence of a robust single-particle excitation gap (measured in STM or ARPES).

### A. Phase pinning by impurities

In realistic systems, impurities [24] or lattice imperfections [20, 21] can pin the density-wave by introducing an excitation gap (i.e., an effective mass) in the phase mode. This excitation gap regularizes the infrared divergence of phase correlations that

underlies the Mermin–Wagner theorem [25–27]. Specifically, as proposed and developed by Fukuyama and Lee [24] as well as by Rice, Whitehouse, and Littlewood [28], the interaction between the density-wave and an impurity potential  $U_i(\mathbf{R} - \mathbf{R}_i)$  located at  $\mathbf{R}_i$  is written as

$$H_i = - \sum_i \int d\mathbf{R} \rho(\mathbf{R}) U_i(\mathbf{R} - \mathbf{R}_i). \quad (\text{S31})$$

Assuming a short-range impurity potential  $U_i(\mathbf{R} - \mathbf{R}_i) = u\delta(\mathbf{R} - \mathbf{R}_i)$  with  $u > 0$ , the action associated with impurity pinning of the density-wave phase becomes

$$S_i = \int dR \left\{ 4uV^{-1} |\Delta_{\mathbf{Q}}| \sum_i \cos[\mathbf{Q} \cdot \mathbf{R}_i + \phi_e(\mathbf{R}_i) + \delta\phi(R)] \right\}, \quad (\text{S32})$$

which implies that the equilibrium phase configuration  $\phi_e$  is no longer spatially uniform, but instead becomes inhomogeneous due to impurity pinning. In the dilute impurity limit, the density-wave locally distorts to maximize its coupling to the impurity potential, leading to the condition [24, 28]

$$\langle \cos[\mathbf{Q} \cdot \mathbf{R}_i + \phi_e(\mathbf{R}_i)] \rangle \approx -1. \quad (\text{S33})$$

As will be shown below, this impurity-induced pinning effectively generates an excitation gap in the phason spectrum, which regularizes the infrared divergence of the phase correlations [29] underlying the Mermin–Wagner theorem [25–27] that forbids long-range ordering in low-dimensional systems.

## B. Dynamics of phase fluctuations

Then, we derive the dynamics of the phase fluctuations in the presence of impurities. Starting from Eqs. (S21) and (S32), the Euler–Lagrange equation with respect to the phase fluctuation field  $\delta\phi$  reads [13]

$$\partial_\mu \left[ \frac{\partial(S_{\text{eff}}^e + S_i)}{\partial(\partial_\mu \delta\phi/2)} \right] = \frac{\partial(S_{\text{eff}}^e + S_i)}{\partial(\delta\phi/2)}, \quad (\text{S34})$$

which leads to the equation of motion

$$\left[ D\partial_t^2 - Df_c(\mathbf{v}_{\mathbf{Q}/2} \cdot \partial_{\mathbf{R}})^2 \right] \frac{\delta\phi(R)}{2} - 8uV^{-1} |\Delta_{\mathbf{Q}}| \sum_i \sin[\mathbf{Q} \cdot \mathbf{R}_i + \phi_e(\mathbf{R}_i) + \delta\phi(R)] = 0. \quad (\text{S35})$$

To proceed, we treat the phase fluctuations within a field-theoretical cumulant expansion, retaining only a single phase operator while contracting the remaining fields. Using the trigonometric identity

$$\sin(\phi_e + \delta\phi) = \sin \phi_e \cos \delta\phi + \cos \phi_e \sin \delta\phi, \quad (\text{S36})$$

and assuming  $\langle \delta\phi \rangle = 0$ , the linear response of the impurity term is governed by the second contribution. The sine of the phase fluctuation is expanded as

$$\sin \delta\phi(R) = \sum_{n=0}^{\infty} \frac{(-1)^n}{(2n+1)!} \delta\phi^{2n+1}(R). \quad (\text{S37})$$

Within the cumulant approximation [6, 7, 13], we retain only a single uncontracted phase operator while contracting the remaining  $2n$  fields according to Wick's theorem [13],

$$\delta\phi^{2n+1}(R) \rightarrow (2n-1)!! \langle \delta\phi^2(R) \rangle^n \delta\phi(R). \quad (\text{S38})$$

Substituting this back, we obtain

$$\begin{aligned} \sin \delta\phi(R) &\rightarrow \sum_{n=0}^{\infty} \frac{(-1)^n}{(2n+1)!} (2n-1)!! \langle \delta\phi^2(R) \rangle^n \delta\phi(R) \\ &= \sum_{n=0}^{\infty} \frac{(-1)^n}{2^n n!} \langle \delta\phi^2(R) \rangle^n \delta\phi(R) = \exp \left[ -\frac{1}{2} \langle \delta\phi^2 \rangle \right] \delta\phi(R). \end{aligned} \quad (\text{S39})$$

Therefore, the impurity term in the linear-response level becomes

$$\sin(\phi_e + \delta\phi) \rightarrow \cos\phi_e \exp\left[-\frac{1}{2}\langle\delta\phi^2\rangle\right]\delta\phi(R). \quad (\text{S40})$$

and then, the equation of motion of the phase fluctuations reads

$$\left\{D\partial_t^2 - Df_c(\mathbf{v}_{\mathbf{Q}/2} \cdot \partial_{\mathbf{R}})^2 - 16uV^{-1}|\Delta_{\mathbf{Q}}| \exp\left[-\frac{1}{2}\langle\delta\phi^2\rangle\right] \sum_i \cos[\mathbf{Q} \cdot \mathbf{R}_i + \phi_e(\mathbf{R}_i)]\right\} \frac{\delta\phi(R)}{2} = 0. \quad (\text{S41})$$

Now, substituting the dilute-impurity condition [24, 28] of Eq. (S33), one finally reaches

$$\left\{D\partial_t^2 - Df_c(\mathbf{v}_{\mathbf{Q}/2} \cdot \partial_{\mathbf{R}})^2 + 16un_iV^{-1}|\Delta_{\mathbf{Q}}| \exp\left[-\frac{1}{2}\langle\delta\phi^2\rangle\right]\right\} \frac{\delta\phi(R)}{2} = 0. \quad (\text{S42})$$

From this equation, the phason energy spectrum follows as

$$\Omega^2(\mathbf{q}) = 16un_i(DV)^{-1}|\Delta_{\mathbf{Q}}| \exp\left[-\frac{1}{2}\langle\delta\phi^2\rangle\right] + f_c(\mathbf{v}_{\mathbf{Q}/2} \cdot \mathbf{q})^2, \quad (\text{S43})$$

or equivalently,

$$\Omega^2(\mathbf{q}) = m_p^2(T) + f_c(\mathbf{v}_{\mathbf{Q}/2} \cdot \mathbf{q})^2, \quad m_p^2(T) = 16un_i(DV)^{-1}|\Delta_{\mathbf{Q}}| \exp\left[-\frac{1}{2}\langle\delta\phi^2\rangle\right]. \quad (\text{S44})$$

Clearly, the impurity-induced pinning effectively generates a finite excitation gap (effective phason mass)  $m_p(T)$  in the phason spectrum. The pinning strength therefore acquires a self-consistent temperature dependence,

$$m_p^2(T) = m_p^2(0) \exp\left[-\frac{1}{2}\langle\delta\phi^2(T)\rangle\right] \frac{|\Delta(T)|}{|\Delta(0)|}, \quad (\text{S45})$$

which explicitly captures the feedback between thermal phase fluctuations and the effective pinning potential: increasing temperature enhances  $\langle\delta\phi^2(T)\rangle$  and reduces  $|\Delta(T)|$ , both of which suppress the coherent impurity pinning and lead to a progressive softening of the phason mode upon warming. To the best of our knowledge, although such a temperature-dependent pinning form has been widely employed at the phenomenological level in the density-wave literature [28, 30], a controlled microscopic derivation starting from an effective action with disorder and phase fluctuations has been lacking. The present work fills this gap by providing a field-theoretical derivation based on the cumulant treatment of phase fluctuations.

### C. Statistic average of phase fluctuations

From the equation of motion of the phase fluctuations in Eq. (S42), the average of thermal phase fluctuations can be obtained within quantum-statistic mechanism [6, 7] either via the fluctuation-dissipation theorem or within the Matsubara formalism. The two approaches are fully equivalent and yield identical results, reflecting the bosonic description of the phase degree of freedom as a collective phason (Nambu–Goldstone [12, 31–33]) mode.

*Fluctuation dissipation theorem.*—Considering the thermal fluctuations, the dynamics of the phase from Eq. (S42) is given by

$$[D\Omega^2(\mathbf{q}) - \omega^2 + iD\omega\gamma] \frac{\delta\phi(\omega, \mathbf{q})}{2} = J_{\text{th}}(\omega, \mathbf{q}). \quad (\text{S46})$$

Here, we have introduced a thermal field  $J_{\text{th}}(\omega, \mathbf{q})$  that obeys the fluctuation-dissipation theorem [34]:

$$\langle J_{\text{th}}(\omega, \mathbf{q})J_{\text{th}}^*(\omega', \mathbf{q}') \rangle = \frac{(2\pi)^3 D \gamma \omega \delta(\omega - \omega') \delta(\mathbf{q} - \mathbf{q}')}{\tanh(\beta\omega/2)}, \quad (\text{S47})$$

and  $\gamma = 0^+$  is a phenomenological damping constant. From this dynamics, the average of the phase fluctuations is given by

$$\begin{aligned} \frac{1}{4}\langle\delta\phi^2\rangle &= \int \frac{d\omega d\omega' d\mathbf{q} d\mathbf{q}'}{(2\pi)^6} \frac{\langle J_{\text{th}}(\omega, \mathbf{q})J_{\text{th}}^*(\omega', \mathbf{q}') \rangle}{D^2[(\omega^2 - \Omega^2(\mathbf{q})) - i\omega\gamma][(\omega'^2 - \Omega^2(\mathbf{q}')) + i\omega'\gamma]} = \int \frac{d\omega d\mathbf{q}}{D(2\pi)^2} \frac{\gamma\omega / \tanh(\beta\omega/2)}{[\omega^2 - \Omega^2(\mathbf{q})]^2 + \omega^2\gamma^2} \\ &= \int \frac{d\mathbf{q}}{(2\pi)^2} \frac{[2n_B(\Omega(\mathbf{q})) + 1]}{2D\Omega(\mathbf{q})}. \end{aligned} \quad (\text{S48})$$

*Matsubara formalism.*—Within the Matsubara formalism, by mapping into the imaginary-time space, from Eq. (S42), the thermal phase fluctuation reads [7]

$$\begin{aligned}
\frac{1}{4}\langle\delta\phi^2\rangle &= \int \frac{d\mathbf{q}}{(2\pi)^2} \left[ \left\langle \left| \frac{\delta\phi^*(\tau, \mathbf{q})}{2} \frac{\delta\phi(\tau, \mathbf{q})}{2} e^{-\int_0^\beta d\tau d\mathbf{q} D \delta\phi^*(\tau, \mathbf{q}) (\Omega^2(\mathbf{q}) - \partial_\tau^2) \delta\phi(\tau, \mathbf{q})/4} \right| \right\rangle \right] \\
&= \int \frac{d\mathbf{q}}{(2\pi)^2} \left[ \frac{1}{Z_0} \int D\delta\phi D\delta\phi^* \frac{\delta\phi^*(\tau, \mathbf{q})}{2} \frac{\delta\phi(\tau, \mathbf{q})}{2} e^{-\int_0^\beta d\tau d\mathbf{q} D \delta\phi^*(\tau, \mathbf{q}) (\Omega^2(\mathbf{q}) - \partial_\tau^2) \delta\phi(\tau, \mathbf{q})/4} \right] \\
&= \int \frac{d\mathbf{q}}{(2\pi)^2} \frac{1}{Z_0} \int D\delta\phi D\delta\phi^* \delta J_q^* \delta J_q e^{-\int_0^\beta d\tau d\mathbf{q} [D \delta\phi^*(\tau, \mathbf{q}) (\Omega^2(\mathbf{q}) - \partial_\tau^2) \delta\phi(\tau, \mathbf{q})/4 + J_q \delta\phi(\mathbf{q})/2 + J_q^* \delta\phi^*(\mathbf{q})/2]} \Big|_{J=J^*=0} \\
&= \int \frac{d\mathbf{q}}{(2\pi)^2} \frac{1}{D} \delta J_q^* \delta J_q \exp \left\{ - \int_0^\beta d\tau \sum_{q'} \frac{1}{\partial_\tau^2 - \Omega^2(\mathbf{q})} J_{q'}^* \right\} \Big|_{J=J^*=0} = - \int \frac{d\mathbf{q}}{(2\pi)^2} \frac{1}{\beta} \sum_{\omega_n} \frac{1}{D} \frac{1}{(i\Omega_n)^2 - \Omega^2(\mathbf{q})} \\
&= \int \frac{d\mathbf{q}}{(2\pi)^2} \frac{2n_B(\Omega(\mathbf{q})) + 1}{2D\Omega(\mathbf{q})}, \tag{S49}
\end{aligned}$$

which is exactly the same as the one in Eq. (S48) obtained via the fluctuation dissipation theorem. Here,  $\Omega_n = 2n\pi T$  represents the Bosonic Matsubara frequencies;  $J_q$  denotes the generating functional and  $\delta J_q$  stands for the functional derivative.

#### SIV. Simulation treatments

Our numerical analysis consists of two complementary steps, which together establish a self-consistent connection between the microscopic band structure and the finite-momentum ordered state.

*Step (I):* First, we construct an effective tight-binding model by fitting to the underlying band structure obtained from our DFT calculation (Fig. 1 in the main text). For each spin component  $s = \pm$ , the electronic dispersion is taken as [35]

$$\xi_{\mathbf{k},s} = -2t(\cos k_x + \cos k_y) - 4t' \cos k_x \cos k_y - 2t_j s_z (\cos k_x - \cos k_y) - \mu, \tag{S50}$$

where  $t$  and  $t'$  denote the nearest- and next-nearest-neighbor hopping amplitudes,  $t_j$  parameterizes the spin-dependent anisotropic term, and  $\mu$  is the chemical potential. From this dispersion, the spin-resolved Fermi momentum  $k_F^s(\theta)$  is determined numerically as a function of the polar angle  $\theta$  along the Fermi surface, defined through the condition

$$\xi_{\mathbf{k},s} \Big|_{\mathbf{k}=k_F^s(\theta)(\cos\theta\hat{\mathbf{e}}_x + \sin\theta\hat{\mathbf{e}}_y)} = 0. \tag{S51}$$

Then, the ordering wave vector for each spin sector is constructed according to

$$\mathbf{Q}_s = 2k_F^s(\theta_{\mathbf{Q}_s}) \left( \cos\theta_{\mathbf{Q}_s} \hat{\mathbf{e}}_x + \sin\theta_{\mathbf{Q}_s} \hat{\mathbf{e}}_y \right), \tag{S52}$$

which corresponds to the dominant  $2k_F$  nesting direction selected by the highly anisotropic Fermi surface. The resulting ordering wave vector  $\mathbf{Q}_s$  is then substituted into the gap equation of Eq. (S26) at zero temperature (ground state), which is solved self-consistently to obtain the magnitude of the order parameter  $|\Delta_{\mathbf{Q}_s}|$  using the underlying tight-binding band structure.

Then, we obtain the spin-resolved density-wave gaps  $|\Delta_{\mathbf{Q}_s}|$  as functions of the ordering direction  $\theta_{\mathbf{Q}_s}$ . The optimal orientation  $\theta_{\mathbf{Q}_s}$  is selected by minimizing the mean-field free energy with respect to  $\theta_{\mathbf{Q}_s}$ . Equivalently, within mean-field theory [6, 7, 36], this procedure amounts to choosing the direction that yields the largest self-consistent gap magnitude,  $|\Delta_s| = |\Delta_{\mathbf{Q}_s}(\theta_{\mathbf{Q}_s})|_{\max}$ , which fixes  $\theta_{\mathbf{Q}_s}$  and hence selects the optimal ordering wave vector  $\mathbf{Q}_s^{\text{op}}$  for each spin sector.

*Step (II):* After identifying the optimal ordering wave vector  $\mathbf{Q}_s^{\text{op}}$  for each spin sector, we substitute  $\mathbf{Q}_s^{\text{op}}$  into the gap equation and evaluate the order-parameter magnitude  $|\Delta(T)|$  using the fitted tight-binding band structure. This procedure yields the full temperature dependence of the density-wave gap and thereby determines all gap-related quantities in a self-consistent manner.

The resulting  $\mathbf{Q}_s^{\text{op}}$  and  $|\Delta(T)|$  are then used as inputs for the temporal stiffness  $D$  [Eq. (S24)] and the condensation fraction  $f_c(T)$  [Eq. (S25)]. With these quantities, we self-consistently evaluate the impurity-induced pinning strength [Eq. (S45)] together with the thermal average of the phase fluctuations  $\langle\delta\phi^2\rangle$ .

Specifically, owing to the Debye–Waller-like exponential structure of the phase-fluctuation renormalization, all zero-point (quantum) fluctuation contributions can be absorbed into the zero-temperature parameters  $m_p(0)$  and  $\rho_{\text{CDW}}(0)$ . Throughout the numerical analysis, we therefore explicitly account only for the thermally excited phase fluctuations,

$$\langle\delta\phi_{\text{th}}^2\rangle/2 = \int \frac{d\mathbf{q}}{(2\pi)^2} \frac{2n_B(\Omega(\mathbf{q}))}{D\Omega(\mathbf{q})}, \tag{S53}$$

where  $\Omega(\mathbf{q}) = \sqrt{m_p^2(T) + f_c(T)} (\mathbf{v}_{Q/2} \cdot \mathbf{q})^2$ . The two-dimensional momentum integral can be decomposed into components parallel and perpendicular to  $\mathbf{v}_{Q/2}$ ,  $\mathbf{q} = q_{\parallel} \hat{\mathbf{v}} + q_{\perp} \hat{\mathbf{v}}_{\perp}$ , with  $\hat{\mathbf{v}} = \mathbf{v}_{Q/2} / |\mathbf{v}_{Q/2}|$ . The integration over the transverse component  $q_{\perp}$  is restricted by a microscopic cutoff  $\Lambda_{\perp}$ . Carrying out the  $q_{\perp}$  integration and introducing the rescaled energy variable  $\bar{E} \equiv |\mathbf{v}_{Q/2}| q_{\parallel}$ , we obtain

$$\frac{\langle \delta\phi_{\text{th}}^2(T) \rangle}{2} = \frac{\Lambda_{\perp}}{2D\pi|\mathbf{v}_{Q/2}|} \int \frac{d\bar{E}}{2\pi} \frac{2n_B \left( \sqrt{m_p^2(T) + f_c(T) \bar{E}^2} \right)}{\sqrt{m_p^2(T) + f_c(T) \bar{E}^2}}. \quad (\text{S54})$$

For the thermal contribution considered here, the integral over  $\bar{E}$  is exponentially convergent due to the Bose distribution function  $n_B(\Omega)$ , which effectively provides a natural high-energy cutoff at  $\Omega \sim T$ .

The specific parameter values employed in the simulations, as well as the criteria used for their selection and experimental fitting, are summarized in Table SI. Within the present framework, only two parameters are not fixed by the microscopic tight-binding band structure and therefore need to be determined by comparison with experiment [37]: the effective interaction strength  $V$  and the transverse momentum cutoff  $\Lambda_{\perp}$ . The inverse coupling  $1/V$  is fixed by fitting the zero-temperature gap magnitude  $|\Delta(T = 0)|$  measured experimentally [37]. Once  $V$  is determined, the full temperature dependence of the gap and the gap-closing temperature  $T_g$  is uniquely fixed within the model. The transverse cutoff  $\Lambda_{\perp}$  primarily controls the phase-fluctuation contribution and hence the temperature  $T_c$  at which the density-wave order parameter  $\rho_{\text{CDW}}(T)$  vanishes. We determine  $\Lambda_{\perp}$  by fitting the experimentally observed disappearance of the density-wave order at  $T_c$  [37].

TABLE SI. Specific parameters used in our numerical calculation. The tight-binding parameters entering the dispersion are obtained by fitting the density-functional-theory band structure and are kept fixed throughout the analysis. The effective interaction strength  $V$  and the transverse momentum cutoff  $\Lambda_{\perp}$ . The inverse coupling  $1/V$  is fixed by fitting the zero-temperature gap magnitude  $|\Delta(T = 0)| = 35$  meV measured experimentally [37]. The transverse cutoff  $\Lambda_{\perp}$  is determined by fitting the experimentally observed disappearance of the density-wave order at  $T_c \sim 100$  K [37]. From a theoretical perspective, the main physical conclusions reported here are robust against moderate variations of the pinning strength  $m_P(0)$  (see Sec. SV A).

tight-binding model parameters (meV)	$t$	$t'$	$t_j$	$\mu$
	90.375	-36.9375	194.24	75.25
model parameter used in gap equation	$ \Delta_s(T = 0) $			
	35 meV			
model parameters used in phase fluctuations	$T_c$	$m_P(T = 0)$		
	100 K	20 meV		

## SV. Discussion of critical behaviors

In this part, we discuss the critical behaviors associated with the phase transitions in our framework.

### A. Density-wave ordering vanishing

We first consider the density-wave ordering transition. Strong phase fluctuations can suppress the long-range density-wave order through thermal averaging even when the gap amplitude remains finite. As a result, the density-wave order parameter vanishes at a lower temperature  $T_c < T_g$ , prior to the closing of the density-wave gap. Within our framework, this suppression is quantitatively captured by the Debye–Waller–like factor  $\exp(-\langle \delta\phi^2 \rangle/2)$  arising from thermal phase fluctuations, which exponentially reduces the coherent density modulation. Consequently, the loss of density-wave order at  $T_c$  is driven by phase disordering rather than by the collapse of the gap amplitude. The intermediate regime  $T_c < T < T_g$  thus corresponds to a pseudogap phase, characterized by a finite gap amplitude but the absence of long-range density-wave order.

Mathematically, the condition  $\exp[-\langle \delta\phi_{\text{th}}^2(T_c) \rangle/2] \ll 1$  has two important consequences.

First, it is equivalent to  $\langle \delta\phi_{\text{th}}^2(T_c) \rangle/2 \gg 1$ , i.e.,

$$\frac{\langle \delta\phi_{\text{th}}^2 \rangle}{2} = \int \frac{d\mathbf{q}}{(2\pi)^2} \frac{2n_B [\sqrt{f_c(T)} (\mathbf{v}_{Q/2} \cdot \mathbf{q})]}{D \sqrt{f_c(T)} (\mathbf{v}_{Q/2} \cdot \mathbf{q})} \Big|_{T=T_c} \gg 1. \quad (\text{S55})$$

Importantly, this condition is independent of the bare pinning scale  $m_p(0)$ , as also proposed in the literature [28, 30]. Therefore, from a theoretical perspective, the transition temperature  $T_c$  is controlled by intrinsic material parameters (such as the electronic structure and phase stiffness) rather than by sample-dependent pinning strength. In this sense,  $T_c$  is expected to be material-dependent but not sample-dependent.

Second, near  $T_c$  where  $m_p(T_c) \simeq 0$ , the absence of an excitation gap in the phason spectrum removes the infrared protection against long-wavelength fluctuations. As a result, the thermal phase fluctuations become strongly enhanced and tend to diverge [see Eq. (S54) with  $m_p = 0$ , which tends to diverge owing to the singularity at  $\tilde{E} = 0$ ], in accordance with the Mermin–Wagner theorem [25–27]. This leads to a detrimental feedback mechanism in the vicinity of  $T_c$ : the suppression of the pinning-induced mass  $m_p(T)$  enhances phase fluctuations, which in turn further suppress  $m_p(T)$  through the Debye–Waller-like renormalization. Consequently, the density-wave order is expected to be rapidly destroyed near  $T_c$ , exhibiting a sharp suppression that resembles a weakly first-order transition.

From a quantum-statistical standpoint, low-dimensional ordering systems are particularly susceptible to thermal fluctuations of the Nambu–Goldstone (phason) mode [12, 31–33], whose infrared divergence precludes spontaneous breaking of continuous symmetries at any finite temperature [29]. Consequently, in the absence of additional symmetry-breaking mechanisms, genuine long-range density-wave order can only emerge in the singular limit  $T = 0$ , where the transition at  $T \rightarrow 0^+$  is intrinsically sharp. In realistic materials, however, disorder [24], lattice commensurability [20, 21], or structural imperfections [20, 21] explicitly lock the density-wave phase, generating a finite gap in the phason spectrum. This pinning regularizes long-wavelength fluctuations and stabilizes density-wave order over a finite temperature range. As temperature increases, thermal activation progressively weakens the effective pinning, leading to a softening of the phason mode. When the pinning scale is sufficiently reduced, fluctuation effects (phason excitations) again become dominant/divergent and destabilize the ordered state. Within this perspective, explicit phase locking converts an otherwise  $T = 0^+$  instability into a transition at a finite critical temperature  $T_c$ , and the mechanism here remains fundamentally consistent with the Mermin–Wagner framework.

## B. Gap closing

We next turn to the gap-closing transition. As mentioned above, once the effective interaction strength  $V$  is fixed by fitting the experimental zero-temperature gap magnitude  $|\Delta_s(T = 0)|$  (which sets the pairing strength in the density-wave channel), the full temperature dependence of the density-wave gap  $|\Delta(T)|$  and hence the gap-closing temperature  $T_g$  are uniquely determined within the model. Since the gap equation is treated at the mean-field level, the gap-closing transition is continuous and exhibits the standard second-order critical behavior. In particular,  $|\Delta(T)|$  vanishes continuously upon approaching  $T_g$  from below, consistent with a mean-field universality class. Notably, in the present work  $2|\Delta(T)|/(k_B T_g) \sim 3.59$ , consistent with the mean-field expectation [6–8].

It is worth emphasizing that the thermal average of the Doppler-shift contribution [3, 4, 16–18],  $\langle (\mathbf{v}_Q/2 \cdot \partial_{\mathbf{R}}\delta\phi/2)^2 \rangle \sim \langle (q_x^2 \delta\phi_{\mathbf{q}}/2)^2 \rangle$  is itself free from infrared divergences. As a result, this quantity does not exhibit the infrared pathology associated with the Mermin–Wagner theorem and therefore does not destabilize the mean-field gap equation in the present continuum setting.

This situation is in clear contrast to lattice-driven density-wave systems, where strong mass renormalization substantially suppresses the phason energy/velocity according to [19–21]

$$\Omega^2(\mathbf{q}) \Rightarrow \frac{m}{m^*} \Omega^2(\mathbf{q}), \quad m/m^* \ll 1, \quad (\text{S56})$$

and hence, amplifies the Doppler-shift effect induced by phase fluctuations. Only in this case, the enhanced feedback of phase fluctuations onto the fermionic spectrum can qualitatively modify the gap equation and can potentially drive the gap-closing transition into a first-order one in the lattice-driven density-wave systems [2].

## SVI. Incommensurate density modulation

A key and intrinsic feature of the density-wave state identified in this work is the incommensurate nature of the ordering wave vectors  $\mathbf{Q}_s^{\text{op}}$ . In the presence of an altermagnetic background, the spin-resolved stripe orders further imply a nontrivial modulation in the spin channel. Specifically, although the primary instability is a spin-conserving density-wave condensation within each spin sector, the superposition of two orthogonal, spin-selective charge modulations naturally produces an antiphase modulation in the spin density, which can be viewed as an emergent SDW-like texture of itinerant electrons. Importantly, this SDW-like modulation is not imposed by a pre-assumed commensurate magnetic unit cell; instead, it is a secondary consequence of the spin-momentum-locked altermagnetic band structure selecting distinct nesting vectors. As a result, the SDW pattern here is generically incommensurate and should be understood as an interference/contrast pattern between two spin-resolved density waves riding on the altermagnetic background. Since  $\mathbf{Q}_s^{\text{op}}$  in a given spin sector is set by the separation between the two

inversion-related open Fermi sheets, which is not symmetry-quantized and depends continuously on band filling, the resulting density modulation is generically incommensurate with the underlying lattice. This incommensurability follows directly from the itinerant, Fermi-surface-driven nature of the instability and does not rely on fine-tuning or additional assumptions.

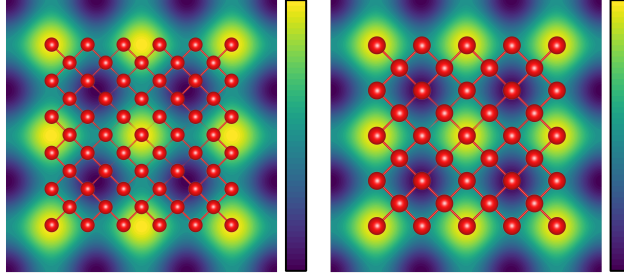


FIG. SI. Real-space spin-density modulation arising from the spin-resolved density-wave state on top of the antiferromagnetic background. Red spheres denote magnetic atoms. Left: density modulation for the chemical potential  $\mu = 0.075$  eV used in the main-text calculations, exhibiting a long-period pattern in which two spin-density modulation oscillations extend over five lattice constants. Right: density modulation for  $\mu = 0.20$  eV, showing a nearly period-doubled modulation in which one spin-density modulation oscillation spans two lattice constants.

For the chemical potential used in the main-text calculations, the real-space modulation (left panel of Fig. SI) exhibits an apparent repetition over a supercell spanning five lattice constants, within which the density wave completes two full oscillation periods. The resulting long-period pattern is thus nearly commensurate over experimentally relevant coherence lengths. Upon a slight adjustment of the chemical potential, the modulation becomes nearly period-doubled (right panel of Fig. SI) and may thus appear “commensurate” in probes with limited momentum resolution. Such rational approximants do not alter the underlying microscopic mechanism and provide a useful description of how an intrinsically incommensurate instability can manifest as an apparently commensurate pattern in real-space imaging or diffraction within finite domains and under weak pinning.

## SVII. Additional discussion of single- $\mathbf{Q}$ SDW

In this part, we briefly discuss the single- $\mathbf{Q}$  SDW scenario within a standard mean-field (Hartree–Fock) framework. For a single- $\mathbf{Q}$  collinear SDW, we start with a standard interacting Hamiltonian [1]

$$H = \sum_{\mathbf{k}, s} \xi_{\mathbf{k}, s} c_{\mathbf{k}s}^\dagger c_{\mathbf{k}s} + \frac{1}{2} \sum_{\mathbf{q}, \sigma_1 \sigma_2 \sigma_3 \sigma_4} U(\mathbf{q}) c_{\mathbf{k}+\mathbf{q}\sigma_1}^\dagger (S_z)_{\sigma_1 \sigma_2} c_{\mathbf{k}\sigma_2} c_{\mathbf{k}'\sigma_3}^\dagger (S_z)_{\sigma_3 \sigma_4} c_{\mathbf{k}'+\mathbf{q}\sigma_4}, \quad (\text{S57})$$

and introduce the longitudinal SDW order parameter [1]

$$\Delta_{\mathbf{Q}} = \frac{U_{\text{SDW}}}{2} m_{\mathbf{Q}}, \quad m_{\mathbf{Q}} = \frac{1}{2} \sum_{\mathbf{k}} \left( \langle c_{\mathbf{k}+\mathbf{Q}, \uparrow}^\dagger c_{\mathbf{k}\uparrow} \rangle - \langle c_{\mathbf{k}+\mathbf{Q}, \downarrow}^\dagger c_{\mathbf{k}\downarrow} \rangle \right), \quad (\text{S58})$$

where  $U_{\text{SDW}} = U(\mathbf{Q})/4$  is the interaction that accounts for the SDW ordering. Performing a Hartree–Fock decoupling in the SDW channel yields the mean-field Hamiltonian [1]

$$H_{\text{MF}} = \frac{1}{2} \sum_{\mathbf{k}} \left[ \xi_{\mathbf{k}\uparrow} c_{\mathbf{k}\uparrow}^\dagger c_{\mathbf{k}\uparrow} + \xi_{\mathbf{k}+\mathbf{Q}, \uparrow} c_{\mathbf{k}+\mathbf{Q}, \uparrow}^\dagger c_{\mathbf{k}+\mathbf{Q}, \uparrow} + (\Delta_{\mathbf{Q}} c_{\mathbf{k}\uparrow}^\dagger c_{\mathbf{k}+\mathbf{Q}, \uparrow} + \text{h.c.}) \right] \\ + \frac{1}{2} \sum_{\mathbf{k}} \left[ \xi_{\mathbf{k}\downarrow} c_{\mathbf{k}\downarrow}^\dagger c_{\mathbf{k}\downarrow} + \xi_{\mathbf{k}+\mathbf{Q}, \downarrow} c_{\mathbf{k}+\mathbf{Q}, \downarrow}^\dagger c_{\mathbf{k}+\mathbf{Q}, \downarrow} - (\Delta_{\mathbf{Q}} c_{\mathbf{k}\downarrow}^\dagger c_{\mathbf{k}+\mathbf{Q}, \downarrow} + \text{h.c.}) \right] + \frac{2|\Delta_{\mathbf{Q}}|^2}{U_{\text{SDW}}}, \quad (\text{S59})$$

where the opposite sign for the two spin sectors reflects that the SDW couples to the spin density (rather than the charge density). Here and below,  $\mathbf{k}$  is understood to be restricted to the reduced Brillouin zone (RBZ) associated with the folding by  $\mathbf{Q}$ . The prefactor 1/2 avoids double counting of the  $(\mathbf{k}, \mathbf{k} + \mathbf{Q})$  pairs when summing over the RBZ.

Diagonalizing  $H_{\text{MF}}$ , we obtain the spin-resolved quasiparticle excitation spectrum

$$E_{\mathbf{k}s}^\pm = \frac{\xi_{\mathbf{k}, s} + \xi_{\mathbf{k}+\mathbf{Q}, s}}{2} \pm E_{\mathbf{k}s}, \quad E_{\mathbf{k}s} = \sqrt{\left( \frac{\xi_{\mathbf{k}, s} - \xi_{\mathbf{k}+\mathbf{Q}, s}}{2} \right)^2 + |\Delta_{\mathbf{Q}}|^2}, \quad s = \uparrow, \downarrow. \quad (\text{S60})$$

Accordingly, one obtains the self-consistent gap equation

$$\frac{2}{U_{\text{SDW}}} = \frac{1}{2} \sum_{\mathbf{k} \in \text{RBZ}} \left[ \frac{f(E_{\mathbf{k}\uparrow}^-) - f(E_{\mathbf{k}\uparrow}^+)}{E_{\mathbf{k}\uparrow}} + \frac{f(E_{\mathbf{k}\downarrow}^-) - f(E_{\mathbf{k}\downarrow}^+)}{E_{\mathbf{k}\downarrow}} \right]. \quad (\text{S61})$$

Then, one should use this combined condition, Eq. (S61), to determine a single SDW gap amplitude  $|\Delta_{\mathbf{Q}}|$  at the same ordering wavevector  $\mathbf{Q}$ .

For a symmetry-related ordering wavevector  $\mathbf{Q}$  (such as  $\mathbf{Q}_0 = (\pi/a, \pi/a)$  considered in previous works [37–39]), the two spin sectors give identical contributions, and hence Eq. (S61) rigorously reduces to the usual compact form,

$$\frac{1}{U_{\text{SDW}}} = \frac{1}{2} \sum_{\mathbf{k} \in \text{RBZ}} \frac{f(E_{\mathbf{k}s}^-) - f(E_{\mathbf{k}s}^+)}{E_{\mathbf{k}s}}, \quad s = \uparrow \text{ or } \downarrow. \quad (\text{S62})$$

It is worth noting that Eq. (S62) is formally identical to the gap equation obtained in the main text for the spin-resolved CDWs. The only essential difference is that, in the single- $\mathbf{Q}$  SDW case considered here, one must require a symmetry-related ordering wavevector  $\mathbf{Q}$  that yields the same self-consistent SDW gap  $|\Delta_{\mathbf{Q}}|$  for both spin sectors. However, as shown in Fig. 2(a) of the main text, there exists essentially no angular window in which both  $|\Delta_{\mathbf{Q}\uparrow}(\theta_{\mathbf{Q}\uparrow})|$  and  $|\Delta_{\mathbf{Q}\downarrow}(\theta_{\mathbf{Q}\downarrow})|$  remain finite simultaneously. In other words, Eq. (S62) admits essentially no solution that allows the system to condense at a common ordering wavevector  $\mathbf{Q}$  and to develop an identical SDW gap magnitude  $|\Delta_{\mathbf{Q}}|$  in both spin sectors.

Physically, this can be attributed to the fact that, for spin-selective and mutually orthogonal quasi-1D open Fermi sheets driven by strong  $d$ -wave altermagnetism, the available phase space for such a common ordering wavevector is highly restricted. In this situation, the spin-up and spin-down electronic sectors reside on distinct, symmetry-inequivalent Fermi-surface segments with different optimal nesting conditions, rendering a simultaneous SDW condensation at the same  $\mathbf{Q}$  energetically unfavorable. As a result, a single- $\mathbf{Q}$  density-wave order involving both spin sectors, i.e., an electronic SDW state modulated at single ordering wave vector without an accompanying charge modulation, is not generically expected in this case.

### SVIII. First-principles calculation method

The first-principles DFT calculations are performed with the projector-augmented-wave method implemented in the Vienna Ab initio Simulation Package (VASP) [40, 41]. We use the Perdew-Burke-Ernzerhof type exchange-correlation functional [42] under the generalized gradient approximation. The cutoff energy of the plane wave basis set is 600 eV. The Brillouin zone is sampled by a Monkhorst-Pack  $k$ -point grids with spacing less than  $0.18 \text{ \AA}^{-1}$ , i.e.,  $9 \times 9 \times 5$ . Atomic structure relaxations were converged to  $1 \mu\text{eV}$  and  $5 \text{ meV}/\text{\AA}$  for energy and forces, respectively. A tighter energy convergence is enforced under  $0.1 \mu\text{eV}$  for the following electronic structure analyses. The effective masses were extracted from parabola fits to the band dispersion dense line sampling along the  $\Gamma - X$  and  $\Gamma - Y$  directions using dense line-mode  $k$ -point sampling near  $\Gamma$ .

---

[1] M. Hoyer and J. Schmalian, Role of fluctuations for density-wave instabilities: Failure of the mean-field description, *Phys. Rev. B* **97**, 224423 (2018).

[2] F. Yang and L. Chen, Microscopic phase-transition theory of charge density waves: revealing hidden transitions of phason and amplitudon, arXiv:2505.05025 (2025).

[3] F. Yang and M. W. Wu, Theory of coupled dual dynamics of macroscopic phase coherence and microscopic electronic fluids: Effect of dephasing on cuprate superconductivity, *Phys. Rev. B* **104**, 214510 (2021).

[4] F. Yang and M. W. Wu, Gauge-invariant microscopic kinetic theory of superconductivity in response to electromagnetic fields, *Phys. Rev. B* **98**, 094507 (2018).

[5] F. Yang and M. W. Wu, Gauge-invariant microscopic kinetic theory of superconductivity: Application to the optical response of Nambu-Goldstone and Higgs modes, *Phys. Rev. B* **100**, 104513 (2019).

[6] G. D. Mahan, *Many-particle physics* (Springer Science & Business Media, 2013).

[7] A. A. Abrikosov, L. P. Gorkov, and I. E. Dzyaloshinski, *Methods of quantum field theory in statistical physics* (Courier Corporation, 2012).

[8] J. Schrieffer, *Theory of Superconductivity* (W.A. Benjamin, 1964).

[9] P. B. Littlewood and C. M. Varma, Gauge-invariant theory of the dynamical interaction of charge density waves and superconductivity, *Phys. Rev. Lett.* **47**, 811 (1981).

[10] I. c. v. Kos, A. J. Millis, and A. I. Larkin, Gaussian fluctuation corrections to the BCS mean-field gap amplitude at zero temperature, *Phys. Rev. B* **70**, 214531 (2004).

[11] S. Fischer, M. Hecker, M. Hoyer, and J. Schmalian, Short-distance breakdown of the Higgs mechanism and the robustness of the BCS theory for charged superconductors, *Phys. Rev. B* **97**, 054510 (2018).

- [12] Y. Nambu, Nobel lecture: Spontaneous symmetry breaking in particle physics: A case of cross fertilization, *Rev. Mod. Phys.* **81**, 1015 (2009).
- [13] M. E. Peskin, *An introduction to quantum field theory* (CRC press, 2018).
- [14] M. Hayashi and H. Yoshioka, Topological dislocations and mixed state of charge density waves, *Phys. Rev. Lett.* **77**, 3403 (1996).
- [15] M. Hayashi and H. Yoshioka, On the ginzburg-landau free energy of charge density waves with a three-dimensional order, arXiv preprint cond-mat/0010102 (2000).
- [16] F. Yang, G. Zhao, Y. Shi, and L. Chen, An efficient phase-transition framework for gate-tunable superconductivity in monolayer wte .2, arXiv:2509.08332 (2025).
- [17] F. Yang, Y. Shi, and L.-Q. Chen, Preformed cooper pairing and the uncondensed normal-state component in phase-fluctuating cuprate superconductivity, arXiv:2509.21133 (2025).
- [18] F. Yang and L. Chen, A tractable framework for phase transitions in phase-fluctuating disordered 2D superconductors: applications to bilayer MoS<sub>2</sub> and disordered InO<sub>x</sub> thin films, arXiv preprint arXiv:2511.13268 (2025).
- [19] P. Lee, T. Rice, and P. Anderson, Conductivity from charge or spin density waves, *Solid State Communications* **14**, 703 (1974).
- [20] G. Grüner, The dynamics of charge-density waves, *Rev. Mod. Phys.* **60**, 1129 (1988).
- [21] G. Grüner and A. Zettl, Charge density wave conduction: A novel collective transport phenomenon in solids, *Physics Reports* **119**, 117 (1985).
- [22] C. Kittel and C.-y. Fong, *Quantum theory of solids*, Vol. 5 (Wiley New York, 1963).
- [23] J. J. Sakurai and J. Napolitano, *Modern quantum mechanics* (Cambridge University Press, 2020).
- [24] H. Fukuyama and P. A. Lee, Dynamics of the charge-density wave. I. impurity pinning in a single chain, *Phys. Rev. B* **17**, 535 (1978).
- [25] P. C. Hohenberg, Existence of long-range order in one and two dimensions, *Phys. Rev.* **158**, 383 (1967).
- [26] N. D. Mermin and H. Wagner, Absence of ferromagnetism or antiferromagnetism in one- or two-dimensional isotropic heisenberg models, *Phys. Rev. Lett.* **17**, 1133 (1966).
- [27] S. Coleman, There are no goldstone bosons in two dimensions, *Commun. Math. Phys.* **31**, 259 (1973).
- [28] T. M. Rice, S. Whitehouse, and P. Littlewood, Impurity pinning of discommensurations in charge-density waves, *Phys. Rev. B* **24**, 2751 (1981).
- [29] A. Auerbach, *Interacting electrons and quantum magnetism* (Springer Science & Business Media, 2012).
- [30] K. Maki, Thermal fluctuations of the order parameter in charge-density waves, *Phys. Rev. B* **33**, 2852 (1986).
- [31] Y. Nambu, Quasi-particles and gauge invariance in the theory of superconductivity, *Phys. Rev.* **117**, 648 (1960).
- [32] J. Goldstone, Field theories with “superconductor” solutions, *Il Nuovo Cimento* **19**, 154 (1961).
- [33] J. Goldstone, A. Salam, and S. Weinberg, Broken symmetries, *Phys. Rev.* **127**, 965 (1962).
- [34] L. D. Landau, E. M. Lifshitz, and L. P. Pitaevskii, *Statistical Physics, Part 1* (Pergamon, New York, 1980).
- [35] L. Šmejkal, A. B. Hellenes, R. González-Hernández, J. Sinova, and T. Jungwirth, Giant and tunneling magnetoresistance in unconventional collinear antiferromagnets with nonrelativistic spin-momentum coupling, *Phys. Rev. X* **12**, 011028 (2022).
- [36] F. Yang and M. W. Wu, Fulde–Ferrell State in Spin–Orbit-Coupled Superconductor: Application to Dresselhaus SOC, *J. Low Temp. Phys.* **192**, 241 (2018).
- [37] B. Jiang, M. Hu, J. Bai, Z. Song, C. Mu, G. Qu, W. Li, W. Zhu, H. Pi, Z. Wei, Y.-J. Sun, Y. Huang, X. Zheng, Y. Peng, L. He, S. Li, J. Luo, Z. Li, G. Chen, H. Li, H. Weng, and T. Qian, A metallic room-temperature *d*-wave altermagnet, *Nat. Phys.* **21**, 754 (2025).
- [38] X. Yan, Z. Song, J. Song, Z. Fang, H. Weng, and Q. Wu, Sdw driven “magnetic breakdown” in a *d*-wave altermagnet KV<sub>2</sub>Se<sub>2</sub>O, arXiv:2505.00074 (2025).
- [39] Y. Xu, H. Zhang, M. Feng, and F. Tian, Electronic structure, magnetic transition, and fermi surface instability of the room-temperature altermagnet KV<sub>2</sub>Se<sub>2</sub>O, *Phys. Rev. B* **112**, 125141 (2025).
- [40] G. Kresse and J. Furthmüller, Efficiency of ab-initio total energy calculations for metals and semiconductors using a plane-wave basis set, *Comp. Mater. Sci.* **6**, 15 (1996).
- [41] G. Kresse and J. Furthmüller, Efficient iterative schemes for ab initio total-energy calculations using a plane-wave basis set, *Phys. Rev. B* **54**, 11169 (1996).
- [42] J. P. Perdew, K. Burke, and M. Ernzerhof, Generalized gradient approximation made simple, *Phys. Rev. Lett.* **77**, 3865 (1996).